

Re-examining the U.K.'s greatest tornado outbreak: forecasting the limited extent of tornadoes along a cold front

Article

Published Version

Apsley, M. L., Mulder, K. J. and Schultz, D. M. (2016) Re-examining the U.K.'s greatest tornado outbreak: forecasting the limited extent of tornadoes along a cold front. *Weather and Forecasting*, 31 (3). pp. 853-875. ISSN 0882-8156 doi: 10.1175/WAF-D-15-0131.1 Available at <https://centaur.reading.ac.uk/61279/>

It is advisable to refer to the publisher's version if you intend to cite from the work. See [Guidance on citing](#).

To link to this article DOI: <http://dx.doi.org/10.1175/WAF-D-15-0131.1>

Publisher: American Meteorological Society

All outputs in CentAUR are protected by Intellectual Property Rights law, including copyright law. Copyright and IPR is retained by the creators or other copyright holders. Terms and conditions for use of this material are defined in the [End User Agreement](#).

www.reading.ac.uk/centaur

CentAUR

Central Archive at the University of Reading

Reading's research outputs online

Reexamining the United Kingdom's Greatest Tornado Outbreak: Forecasting the Limited Extent of Tornadoes along a Cold Front

MIRIAM L. APSLEY,^a KELSEY J. MULDER, AND DAVID M. SCHULTZ

Centre for Atmospheric Science, School of Earth, Atmospheric and Environmental Sciences, University of Manchester, Manchester, United Kingdom

(Manuscript received 5 October 2015, in final form 28 March 2016)

ABSTRACT

On 23 November 1981, a strong cold front swept across the United Kingdom, producing tornadoes from the west to the east coasts. An extensive campaign to collect tornado reports by the Tornado and Storm Research Organisation (TORRO) resulted in 104 reports, the largest U.K. outbreak on record. The front was simulated with a convection-permitting numerical model down to 200-m horizontal grid spacing to better understand its evolution and meteorological environment. The event was typical of tornadoes in the United Kingdom, with convective available potential energy (CAPE) less than 150 J kg^{-1} , 0–1-km wind shear of $10\text{--}20 \text{ m s}^{-1}$, and a narrow cold-frontal rainband forming precipitation cores and gaps. A line of cyclonic absolute vorticity existed along the front, with maxima as large as 0.04 s^{-1} . Some hook-shaped misovortices bore kinematic similarity to supercells. The narrow swath along which the line was tornadic was bounded on the equatorward side by weak vorticity along the line and on the poleward side by zero CAPE, enclosing a region where the environment was otherwise favorable for tornadogenesis. To determine if the 104 tornado reports were plausible, first possible duplicate reports were eliminated, resulting in as few as 58 tornadoes to as many as 90. Second, the number of possible parent misovortices that may have spawned tornadoes is estimated from model output. The number of plausible tornado reports in the 200-m grid-spacing domain was 22 and as many as 44, whereas the model simulation was used to estimate 30 possible parent misovortices within this domain. These results suggest that a number of 90 reports was plausible.

1. Introduction

On 23 November 1981, a strong cold front swept across the United Kingdom, producing an unprecedented 104 reports of tornadoes (Fig. 1). Called Britain's greatest tornado outbreak (Rowe and Meaden 1985), this event had many more tornadoes than the next largest event just a month earlier on 20 October 1981, which spawned only 29 tornadoes (Turner et al. 1986; Rowe 2016). For comparison, even modest outbreaks by U.S. standards are

relatively uncommon in the United Kingdom. Specifically, over 90% of U.K. tornado days between 1980 and 2012 had fewer than eight tornadoes (Fig. 14 in Mulder and Schultz 2015). The November 1981 outbreak is so exceptional that it distorts the historical record and climatologies of tornadoes in the United Kingdom and Europe. For example, in the U.K. tornado climatology by Mulder and Schultz (2015), several figures had to be plotted with the outbreak excluded (e.g., their Figs. 5–7, 9, 12, and 13), and, in their review of tornadoes across Europe, Antonescu et al. (2016) found that the large number of reports produced a bias in their synthesized results and capped the total number of reports from this outbreak at 58. Given the large number of reports distorting the climatologies and that a scientific study of this event has not been performed in nearly 35 years, we believe that the time is right to reexamine this event.

The locations of these 104 reports (Fig. 1) come from the Tornado and Storm Research Organisation (TORRO). TORRO is a U.K.-based not-for-profit organization responsible for collecting tornado reports

 Denotes Open Access content.

^a Additional affiliation: Christ's College, University of Cambridge, Cambridge, United Kingdom.

Corresponding author address: Prof. David M. Schultz, Centre for Atmospheric Science, School of Earth, Atmospheric and Environmental Sciences, University of Manchester, Simon Building, Oxford Road, Manchester M13 9PL, United Kingdom.
E-mail: david.schultz@manchester.ac.uk

DOI: 10.1175/WAF-D-15-0131.1

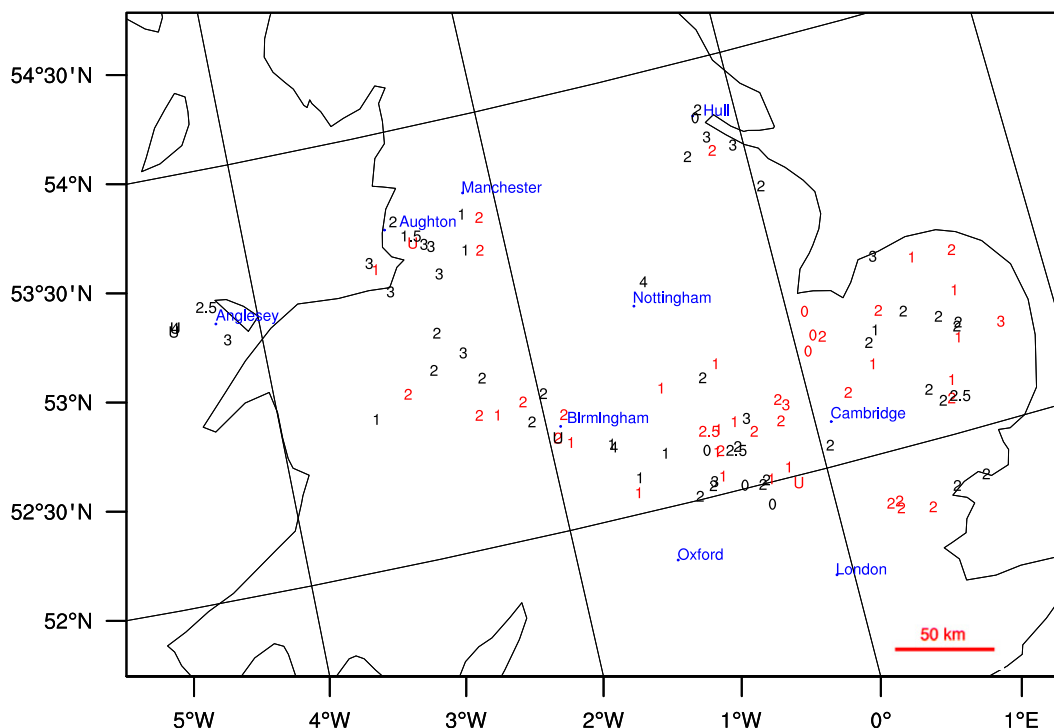


FIG. 1. Locations of the 104 tornado reports from the TORRO database for 23 Nov 1981. Numbers represent their strength on the T scale, U represents unknown intensity, and half values represent intensities between two classes (e.g., 2.5 represents T2–T3). Reports verified by TORRO (58) are classified as definite and plotted in black. Reports that have not been verified (46) are classified as probable and are plotted in red. Locations discussed in the text are labeled in blue. Locations of reports that appear to be located over water are a result of a coarse representation of geography.

from the media, from over 350 observers in the United Kingdom, and from the public through TORRO's website (<http://www.torro.org.uk>) (e.g., [Elsom et al. 2001](#); [Doe 2016](#)). Of the 104 reports on 23 November 1981, 35 came from media reports, 30 came from the public after a call for reports on Anglia Television, and 39 were the result of TORRO's appeal in local newspapers ([Rowe 1985](#)). The challenges of severe-weather event verification can be immense, even when events are well observed by expert meteorologists ([Speheger et al. 2002](#); [Trapp et al. 2006](#)). The challenges are compounded when reports are collected well after the event from primarily nonmeteorologists, as was the case in this event.

The first tornadoes of the day occurred in Anglesey, on the west coast of Wales ([Fig. 1](#)), where there were five reports around 1000 UTC; 20 houses were damaged there, and a summer house (comparable to a small temporary building or mobile home) was turned upside down ([Kemp and Morris 1982](#)). The next seven tornado reports occurred near Aughton (near Liverpool) at 1100 UTC, and there were four more in greater Manchester at 1200 UTC. A further 11 reports in the early afternoon came from

Birmingham, Nottinghamshire, and the East Midlands (east of Birmingham), where 20 large caravans (camper vans) were blown over ([Rowe and Meaden 1985](#)). Seven tornado reports clustered near Hull in the early afternoon. Many of the reports (43), however, came from East Anglia (northeast of Cambridge) between 1300 and 1600 UTC. The last tornadoes occurred in southeast Essex (east-northeast of London) just before 1600 UTC.

Despite the large number of reports and despite occurring in conjunction with an extensive southwest–northeast-oriented cold front advancing southeastward across nearly the entirety of the United Kingdom, these tornado reports only occurred along a narrow swath 200–250 km wide and 400 km long ([Fig. 1](#)). Thus, the first goal of this article is to determine why the tornadoes occurred in a narrow swath along an otherwise extensive cold front.

There are few exact details given with most of the tornado reports, so the duration of each tornado is unknown; some eyewitnesses, however, estimated lifetimes of 20–30 s or less ([Rowe 1985](#)). Eight tornado reports included damage track lengths between 0.3 and 4 km long. Where estimated, damage tracks are believed

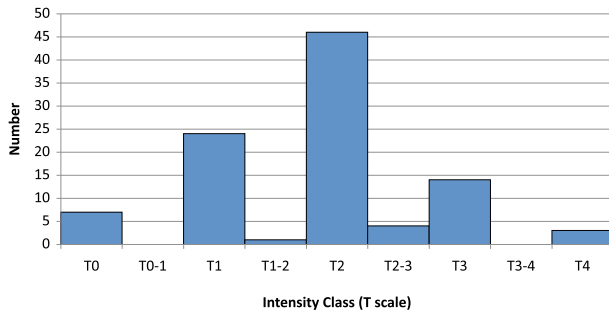


FIG. 2. Distribution on the T scale of intensities of the 99 tornado reports on 23 Nov 1981 associated with an intensity rating from the TORRO database.

to have had widths of 10–20 m. The direction of travel was reported in 16 cases, with 14 coming from between west and north-northwest, consistent with the movement of the front; the other 2 came from the south and southwest. Ninety-nine of the 104 reports were assigned values on the International Tornado Intensity Scale or T scale (Meaden 1983; Meaden et al. 2007). Compared to the Fujita (F) scale, the T scale has twice as many classifications. Conversion between the F and T scales can be performed using the equation $F \approx 0.5T$ and rounding down to the nearest integer (Brooks and Doswell 2001; Meaden et al. 2007). Figure 2 shows that most (96, or 97%) of the tornadoes were T0–T3 (or F0–F1); three tornadoes, however, reached T4 (or F2). This distribution is similar to the national distribution from the Kirk (2014) and Mulder and Schultz (2015) climatologies in which 94%–95% were between T0 and T3 (or F0–F1).

Because tornado reporting in this event relied on responses from a media campaign, the figure of 104 tornado reports has been controversial. Extrapolating based on the density of reports and the sparsely populated areas over which most of the cold front traveled, Rowe and Meaden (1985) suggested that the number of tornadoes may possibly have been as high as 400–500. On the other hand, only 58 of these reports (56% of the 104 reports) were later verified by TORRO experts according to the TORRO database and classified as definite; the other 46 reports were deemed to show reasonable evidence of a tornado having occurred, but not enough to be certain; these were classified as probable. Thus, the lack of confirmation of nearly half of the reports and the extreme magnitude of the outbreak in the historical context suggest that the 104 reports might be an overestimate.

In this article, we use two different approaches to investigate the tornado reports. First, we undertake a reexamination of the individual tornado reports for the possible occurrence of multiple reports of the same

tornado. Second, we use a cloud-resolving model to simulate the cold front and possible parent circulations to the tornadoes. The number of parent circulations might give us some insight into the number of tornadoes. Thus, the second goal of this article is to reexamine the tornado reports and the meteorological conditions on that day to see if we can constrain the minimum and maximum numbers of tornadoes that likely occurred.

2. Background on tornadoes along cold fronts

Tornadoes forming along cold fronts are a challenging forecasting problem. Such tornadoes are often associated with a class of convective storms occurring along cold fronts called narrow cold-frontal rainbands. Narrow cold-frontal rainbands have been described by Browning and Harrold (1970), Browning and Pardoe (1973), Carbone (1982), Hobbs and Persson (1982), Browning and Reynolds (1994), Browning and Roberts (1996), Browning et al. (1997), Jorgensen et al. (2003), and Viale et al. (2013), among many others. Narrow cold-frontal rainbands have been synthesized by conceptual models in Browning (1990) and Houze (2014, section 11.4.4). In the United States, narrow cold-frontal rainbands are a subset of what have been termed quasi-linear convective storms (QLCSs; Trapp et al. 2005). Trapp et al. (2005) applied this term for their investigation of tornadoes that form along such line convection (i.e., distinct from supercell convective storms).

Tornadoes along linear convective systems are challenging because they tend to have shorter lead times than tornadoes associated with supercells (Trapp et al. 2005). Even if the specific location and timing of the tornadoes cannot be predicted well in advance, predicting the general location along the line where tornadoes form would be an operationally useful tool. Indeed, Atkins et al. (2004) showed that tornadoes were more likely to form from parent mesovortices along the convective line that had greater rotation rates, implying that the strongest vortices may favor tornadogenesis.

Before discussing how tornadoes form along linear convective storms, we need to distinguish between the parent circulations that precede the tornadoes and the tornadoes themselves. One of the characteristics often observed in narrow cold-frontal rainbands is the presence of precipitation cores and gaps, aligned anticyclonically relative to the front. These core-and-gap regions have been reported for cold fronts over the eastern North Pacific Ocean (e.g., Hobbs and Biswas 1979; Hobbs and Persson 1982; Jorgensen et al. 2003), near the Alps (Hagen 1992), over eastern North America and the Atlantic Ocean (Locatelli et al. 1995; Wakimoto and Bosart 2000), and over the United

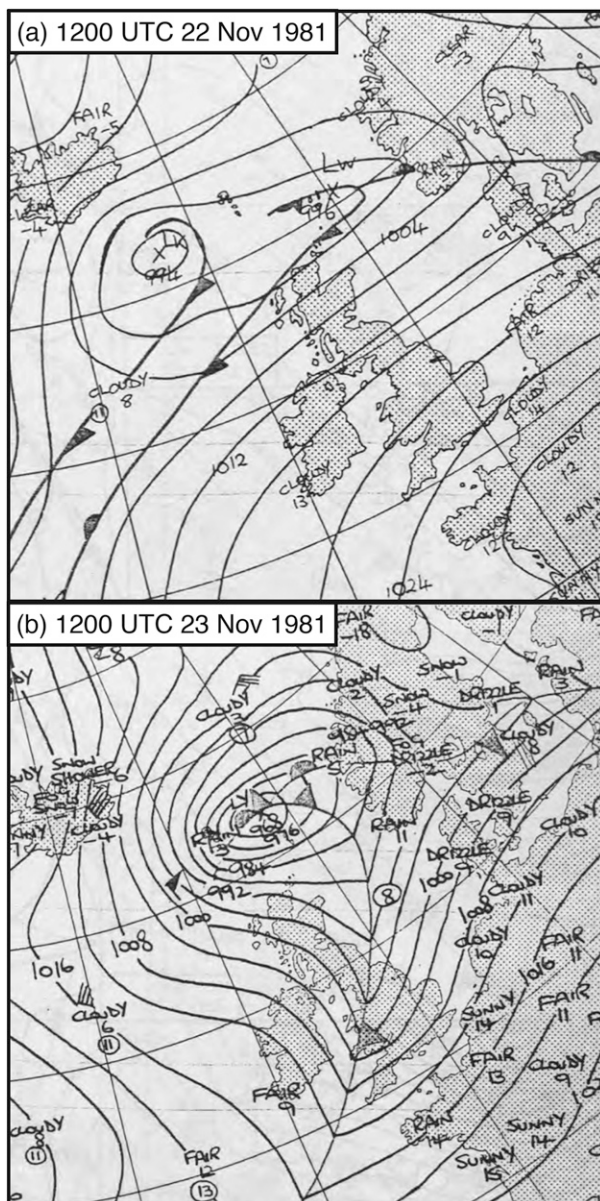


FIG. 3. Excerpts from Met Office Daily Weather Summary surface weather charts at (a) 1200 UTC 22 Nov and (b) 1200 UTC 23 Nov 1981. Plotted are sea level pressure contours every 4 hPa, surface fronts, surface temperatures ($^{\circ}\text{C}$) and weather at selected cities, and occasionally wind barbs (standard notation). (Crown copyright.)

Kingdom (e.g., James and Browning 1979; Browning and Roberts 1996). Specifically, other tornadic cold fronts in the United Kingdom also possessed this core-and-gap structure (e.g., Smart and Browning 2009; Clark and Parker 2014; Mulder 2015), as well as in Japan (e.g., Kobayashi et al. 2007; Sugawara and Kobayashi 2009).

The cores are often associated with heavier precipitation and relative maxima in vorticity (hereafter misovortices),

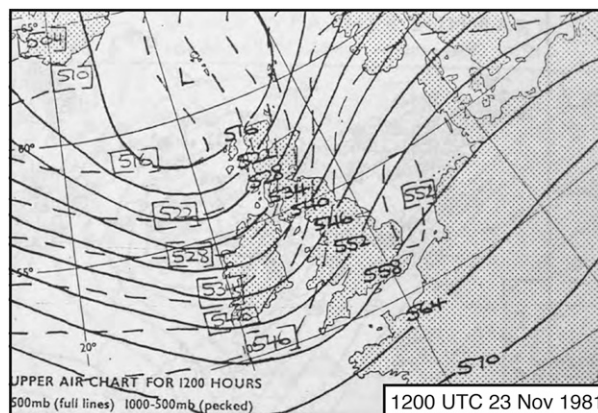


FIG. 4. Excerpt from Met Office Daily Weather Summary 500-hPa chart at 1200 UTC 23 Nov 1981. Plotted are 500-hPa geopotential height (solid lines every 6 dam) and 1000–500-hPa thickness (dashed lines every 6 dam). (Crown copyright.)

whereas the gaps are associated with weaker precipitation or the absence of precipitation and relative minima in vorticity. Misovortices have diameters of 1–4 km (Fujita 1981) and have been suggested to be the parent circulation from which the tornadoes form. Different explanations have been offered to explain misovortex formation, including the release of horizontal shearing instability (e.g., Carbone 1982; Hobbs and Persson 1982; Lee and Wilhelmson 1997b; Jorgensen et al. 2003; Wheatley and Trapp 2008; Kawashima 2011), advection of hydrometeors (Locatelli et al. 1995), trapped gravity waves (Brown et al. 1999), tilting of vorticity along the cold front (Carbone 1983), or combinations of the above.

How tornadoes form along linear convective storms is less well known compared to supercellular tornadoes, primarily because detailed field observations of tornadoes forming along linear convective storms have not been collected and because of the large computational expense of producing a tornado within a numerical model. Because of the shorter lead time and the different parent-storm morphology to supercells, Trapp et al. (1999) suggested that a different tornadogenesis mode may be responsible for tornadoes from linear convective systems than tornadoes from supercells. Carbone (1983) found that the downdraft was coincident with the tornado, suggesting the importance of tilting and a similarity with tornadogenesis in supercells. In contrast, Lee and Wilhelmson (2000) found the importance of the stretching of strong initial vorticity in their simulations of non-supercell tornadogenesis. Nevertheless, the data and simulations in this article will be insufficient to address the issue of tornadogenesis in this case. Thus, we focus on the misocyclones, the locations of the tornadoes, and an approach to forecasting the occurrence of tornadoes along

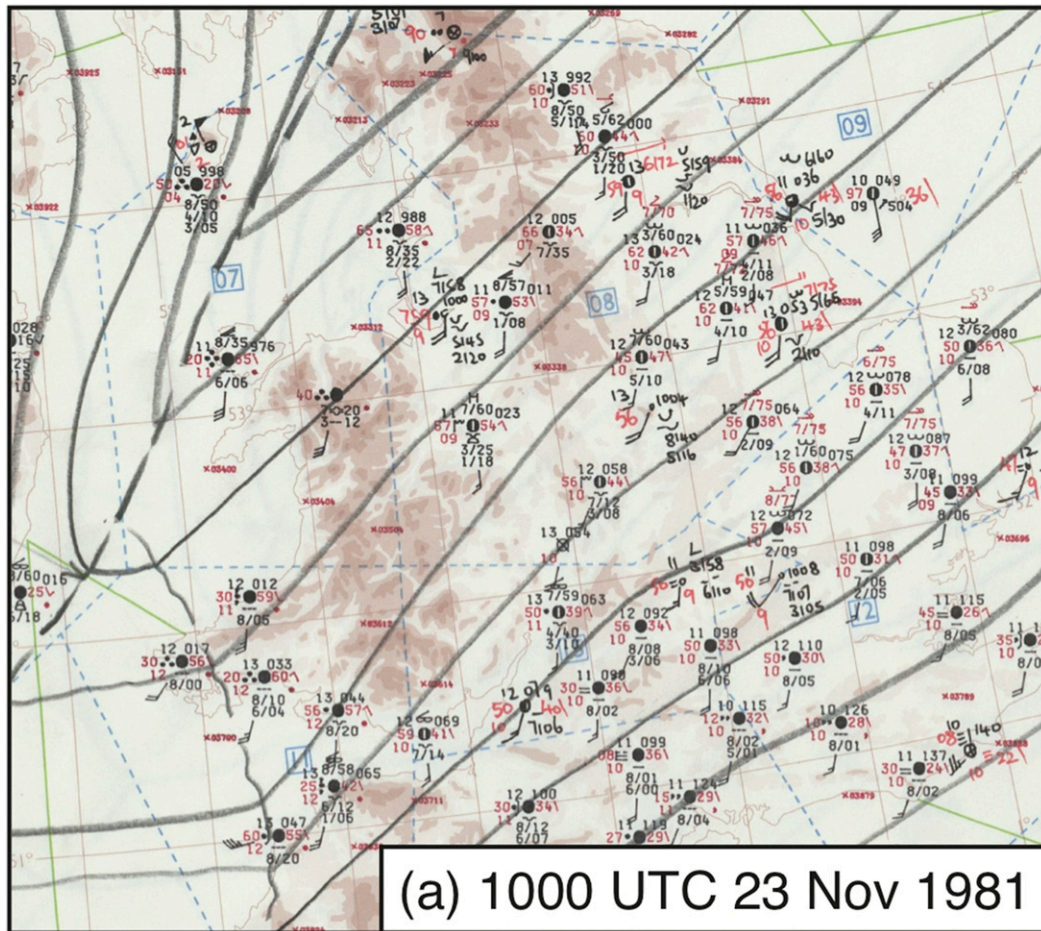


FIG. 5. Excerpts from the Met Office Central Forecasting Office hourly U.K. working charts at (a) 1000 UTC 23 Nov 1981. Plotted are sea level pressure (solid lines every 2 hPa), cold front (dashed line), and standard station models. (Crown copyright.)

lines, as demonstrated for the case of Britain's greatest tornado outbreak on 23 November 1981.

3. Observations: Synoptic and mesoscale overview

At 1200 UTC 22 November 1981, archived Met Office charts identified a broad region of low pressure with two centers of 994 and 996 hPa centered southeast of Iceland and north of the United Kingdom (Fig. 3a). Twelve hours later, the cyclone consolidated with a central pressure of 986 hPa (not shown). By 1200 UTC 23 November, the low had rapidly deepened another 18 hPa to 968 hPa and was moving toward Norway (Fig. 3b), making landfall by 0600 UTC 24 November with a central pressure of 959 hPa (not shown). The cyclone was associated with a sharp trough in 500-hPa geopotential height and strong geostrophic cold advection in the lower troposphere, as indicated by the 1000–500-hPa thickness contours (Fig. 4).

Associated with this cold advection was a strong cold front at the surface. Archived hourly Met Office surface maps show the front extending to the south of the cyclone across the United Kingdom and its southeastward progression (Fig. 5). As the cold front crossed England and Wales, temperatures fell by 6°–7°C in the first hour, and the pressure rose by as much as 4–5 hPa in the first hour after frontal passage and 3 hPa h^{−1} thereafter (Rowe and Meaden 1985; Fig. 5). The wind direction veered suddenly from 190°–230° before the front, a direction roughly parallel to the front, to 320°–340° after the front, a postfrontal direction nearly perpendicular to the orientation of the front (e.g., Fig. 5c). By 1800 UTC, the cold front had cleared England and moved over the North Sea (Rowe 1985; Rowe and Meaden 1985). Moderate rain preceded and was associated with the front in northwestern England at the hour ending 1200 UTC (as much as 10 mm h^{−1}; Fig. 6). The infrared

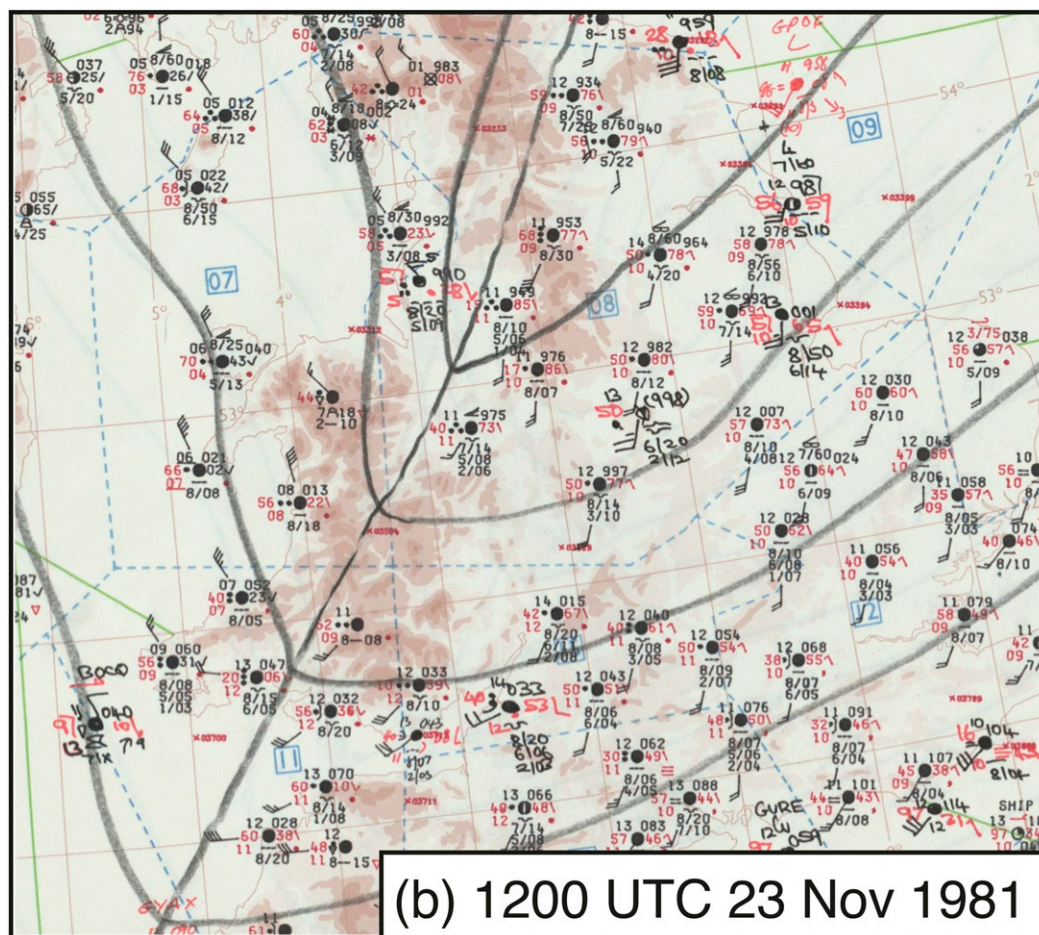


FIG. 5b. As in (a), but for 1200 UTC with sea level pressure plotted every 4 hPa.

satellite image at 1325 UTC (Fig. 7) showed the low center to the north of the United Kingdom and the broad band of clouds associated with the cold front and a prefrontal band. As the front moved southeastward into central England, the precipitation weakened dramatically to less than 2 mm h^{-1} during the hour ending at 1400 UTC (Fig. 6).

Unfortunately, none of the operational soundings that day were ideal for sampling the prefrontal air. The nearest proximity sounding occurred at Aughton near Liverpool, about 11 h before frontal passage at 0000 UTC (Fig. 8). This sounding exhibited only 13 J kg^{-1} convective available potential energy (CAPE), a steep lapse rate between 850 and 700 hPa, and a strong 60-kt (31 m s^{-1}) westerly wind at 850 hPa (Fig. 8). A sounding from the NCEP–NCAR reanalysis (Kalnay et al. 1996) for a location in western England (52.5°N , 2.5°W) at 1200 UTC 23 November had a surface-based CAPE of 147 J kg^{-1} , which is only slightly higher than the $50\text{--}100 \text{ J kg}^{-1}$ of CAPE from the model simulation initialized from the

European Centre for Medium-Range Weather Forecasts (ECMWF) reanalyses (jump ahead to Fig. 13).

These conditions—strong cold front, small CAPE, prefrontal winds nearly parallel to the front, and post-frontal winds nearly perpendicular to the front—are consistent with weather conditions associated with other tornado outbreaks in the United Kingdom (e.g., Bolton et al. 2003; Holden and Wright 2004; Clark 2009, 2013; Clark and Parker 2014; Mulder 2015). Given the synoptic situation, the morphology of the convective storm (also called its convective mode) is likely consistent with previous tornadic convective storms over the United Kingdom, which tend to occur along cold fronts in linear convective storms. Linear convective storms account for 42% of the tornadoes and 51% of the tornado outbreaks in the United Kingdom (Mulder and Schultz 2015), unlike in the United States where linear storms account for only 18%–25% of the tornadoes (Trapp et al. 2005; Smith et al. 2012). [In comparison, supercells produce 79% of U.S. tornadoes (Trapp et al. 2005).] Clark (2013)

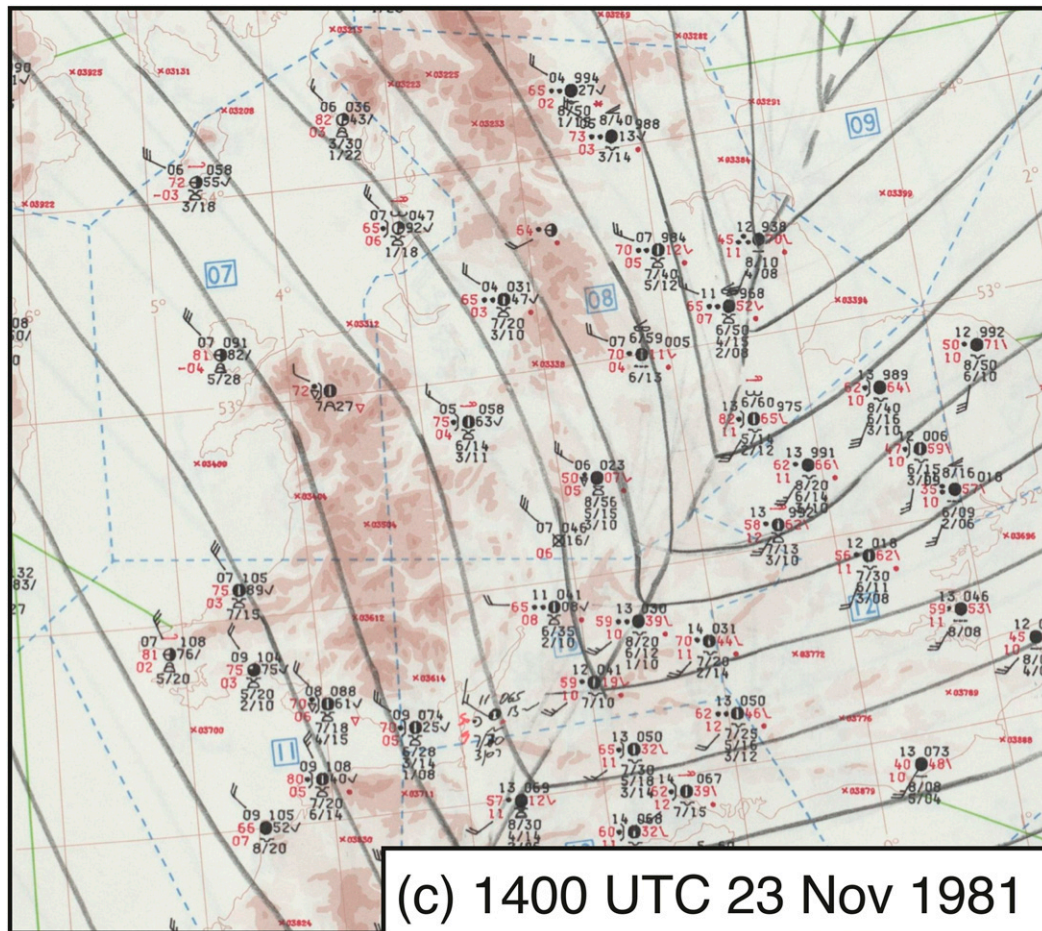


FIG. 5c. As in (a), but for 1400 UTC.

examined 103 convective lines in the United Kingdom and found that 27% were associated with at least one tornado, further evidence for the importance of these lines in producing tornadoes in this region.

Because radar data for this event (Doppler winds or even reflectivity) are unavailable, the precipitation structure of the cold front on that day is unknown. Therefore, we investigate this event further with a model simulation.

4. Model simulation: Setup

As has been demonstrated for other cases, model simulations can be an effective tool for understanding tornadic fronts in the United Kingdom (e.g., [Smart and Browning 2009](#); [Groenemeijer et al. 2011](#); [Mulder 2015](#)). Therefore, we performed a convection-permitting simulation to construct a four-dimensionally consistent dataset to explore a likely meteorological evolution for this event. A successful simulation would be useful for examining the conditions favorable for the tornadoes

within the narrow swath and help interpret the 104 reports of tornadoes.

The simulation was performed using the Advanced Research version of the Weather and Forecasting Model, version 3.4.1 (ARW; [Skamarock et al. 2008](#)). The simulation was initialized at 0600 UTC 23 November 1981 from the ECMWF reanalysis at $0.25^\circ \times 0.25^\circ$ grid spacing interpolated onto a Lambert conformal grid. Lateral boundary conditions were provided by the ECMWF reanalyses every 6 h. Otherwise, the simulation was set up exactly the same as that in [Mulder \(2015\)](#) for the more modest U.K. tornado outbreak of 29 November 2011, which featured seven reported tornadoes across Wales and northern England. The simulation featured 90 vertical levels and four domains, ranging from the outermost domain with 25-km horizontal grid spacing, to three two-way nested domains of 5-km, 1-km, and 200-m horizontal grid spacing (the innermost two domains are shown in [Fig. 9](#)). Even at 200-m grid spacing, the model would have been

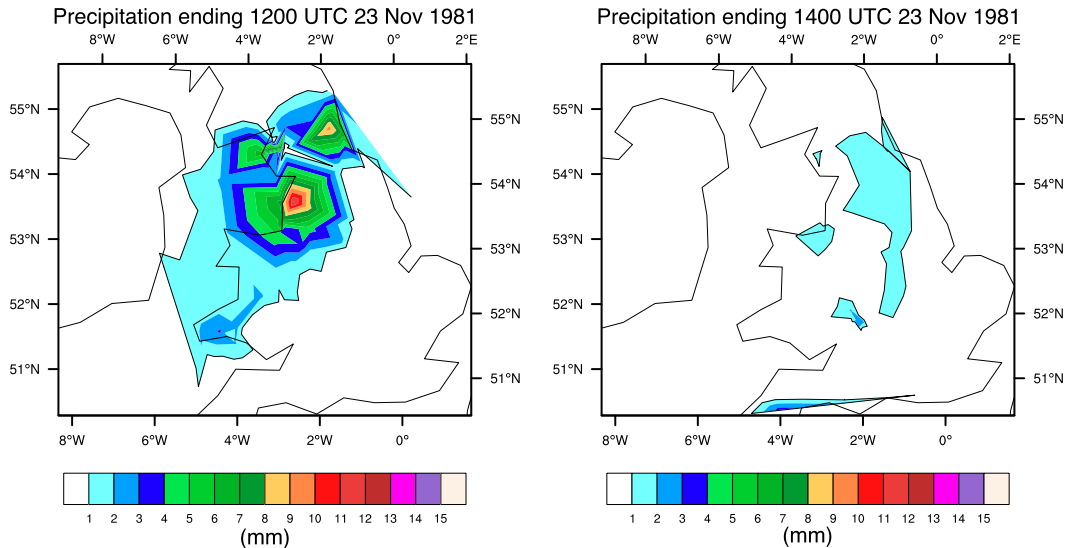


FIG. 6. Hourly rainfall amounts (mm) from (left) 213 rain gauges ending at 1200 UTC and (right) 212 rain gauges ending at 1400 UTC 23 Nov 1981.

inadequate to resolve any possible tornadoes. Instead, the innermost domain is analyzed for the existence of misocyclones, small-scale circulations along linear convective systems that may precede tornadoes. Only output from the 1-km and 200-m domains is shown in the present article. Model output was saved for further diagnosis every 30 min for the 1-km domain and every 10 s for the 200-m domain.

The Kain–Fritsch convective parameterization (Kain and Fritsch 1990; Kain 2004) was employed on the outermost 25-km domain only. Other physical parameterizations included the five-layer thermal diffusion land surface scheme (Skamarock et al. 2008, their section 8.4.1), Thompson et al. (2008) cloud microphysics, and the Mellor–Yamada–Janjić boundary layer (Mellor and Yamada 1982; Janjić 1994, 2002). These parameterizations were chosen because Mulder (2015) found that they produced the most successful simulation of her case. Testing three different microphysical parameterizations [WRF single-moment 6-class scheme; Morrison et al. (2009); Thompson et al. (2008)] did not produce different structures for the core-and-gap regions along the cold front in this case.

5. Model simulation: Mesoscale analysis

The meteorology on the 1-km domain is presented in this section. Subsequent analysis in this article occurs at 1000 UTC, around the time the first tornadoes were reported in Anglesey, and at 1400 UTC, just before the majority of tornadoes were reported in East Anglia. To illustrate the intensity of the front, surface temperature,

wind, and sea level pressure at 1000 and 1400 UTC are presented in Fig. 10. The passage of the front was associated with a sharp pressure trough, a temperature drop of 6°–8°C, and nearly a 90° veering of the wind (Fig. 10). The winds on either side of the front changed direction from 180°–230° on the warm side to 310°–330° on the cold side, although the wind speeds were roughly the same across the front at about 5–10 m s^{−1}. The

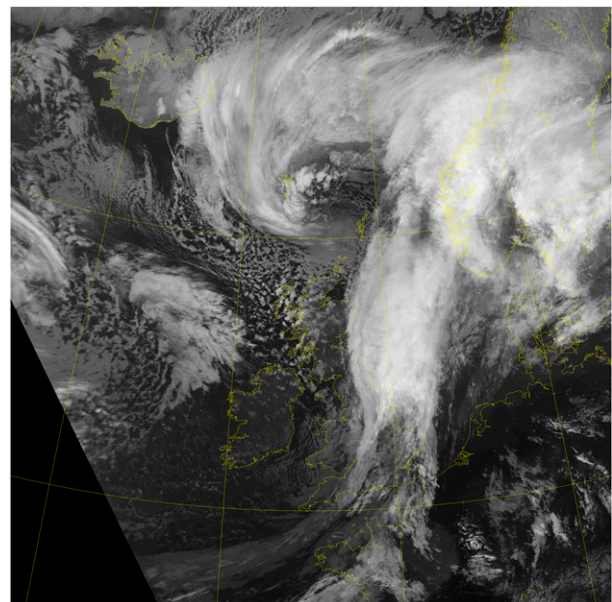


FIG. 7. Infrared satellite imagery (channel 5, 11.5–12.5 μm) at 1325 UTC 23 Nov 1981. (Courtesy of Dundee Satellite Receiving Station.)

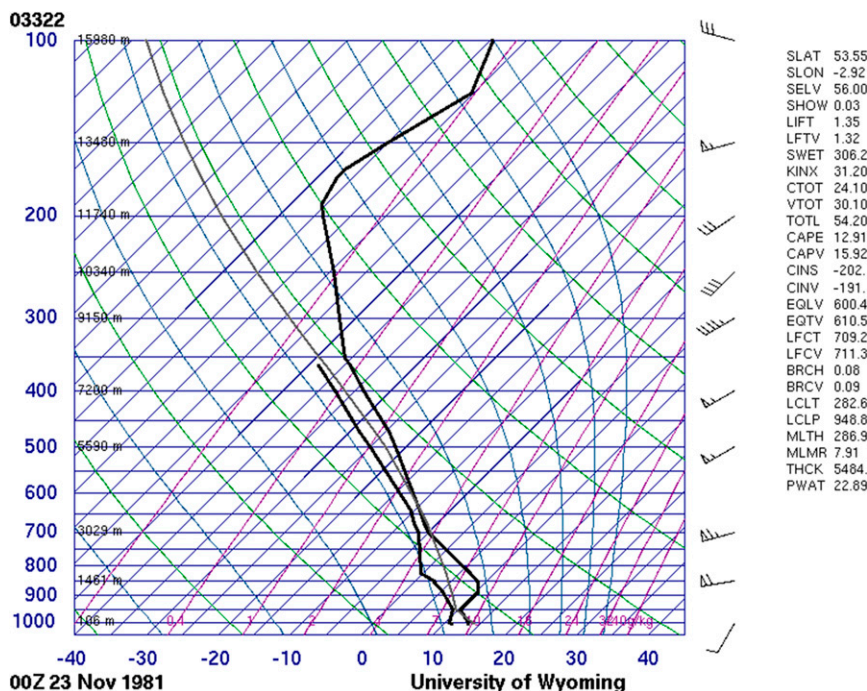


FIG. 8. Prefrontal sounding from Aughton, near Liverpool, at 0000 UTC 23 Nov 1981.
(Courtesy of the University of Wyoming; <http://weather.uwyo.edu/upperair/sounding.html>.)

simulation is consistent with the observations reported in section 3, except for its being an hour behind the observations (cf. Figs. 5a and 10a; cf. Figs. 5c and 10b).

At 1000 UTC 23 November, the simulated radar reflectivity factor reveals poorly organized precipitation along the pressure trough over most of the domain, with reflectivities of up to 45 dBZ, ahead of the wind shift along the cold front around the time the band first arrived in the United Kingdom (Fig. 11a). Along the cold front in the northwest part of the domain, a shorter, narrower, more organized, and more intense (45–50 dBZ) line of convection developed (Fig. 11a). As the rainband progressed across the United Kingdom, the areal coverage of the precipitation decreased as the alongfront extent of the rainband increased, consistent with the observations (cf. Figs. 6 and 11). In particular, as the line passed over the Pennine mountain range in the center of northern England, much of the precipitation weakened, and the band split into a higher reflectivity line positioned along the front and a line of precipitation tens of kilometers ahead of the front (Fig. 11b). The observed counterpart to the modeled prefrontal band, although present in the satellite imagery (Fig. 7 at 1325 UTC), did not appear to produce any measurable precipitation at the rain gauges (Fig. 6 during 1300–1400 UTC). Whether this is because the band was poorly forecast or the stations did not receive rain is unclear at this time. In any case, this prefrontal band is

not the focus of the article, as it is not associated with the formation of the tornadoes. At maturity of the convective line, cores of stronger precipitation became separated by gaps of about 10 km in length of lighter or no precipitation, similar to previously published work summarized in section 2.

The front was associated with a line of absolute vorticity maxima at 500 m above sea level (ASL), which was strongest to the north and weakest to the south (Fig. 12)

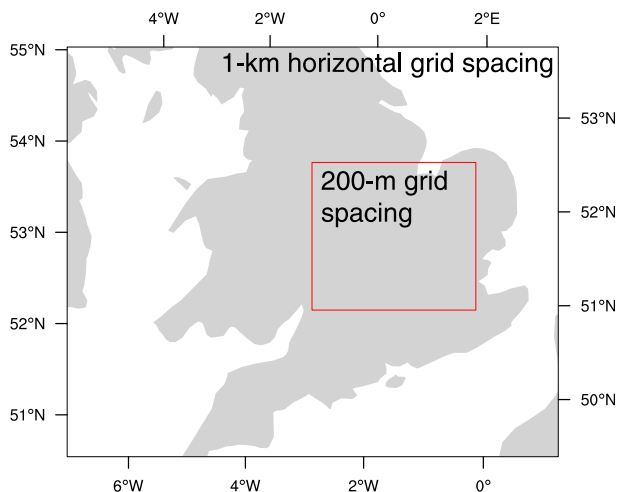


FIG. 9. The two innermost domains used in this simulation.

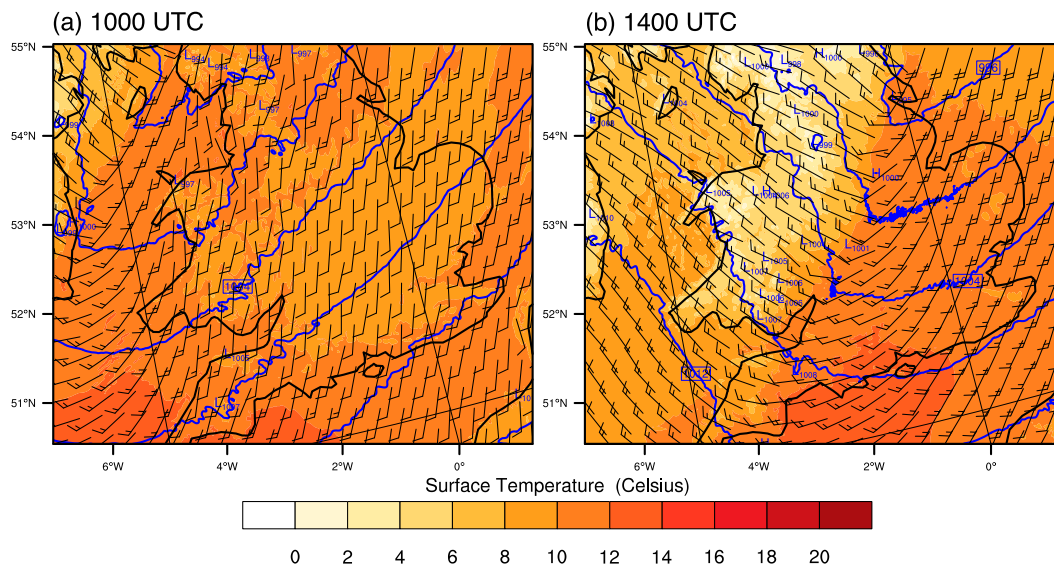


FIG. 10. Simulation of sea level pressure (hPa; blue lines), surface temperature (°C; colored according to scale), and surface winds (pennant; full barb, and half barb denote 25, 5, and 2.5 m s⁻¹, respectively; separation between displayed wind vectors is 30 km) on the domain with 1-km horizontal grid spacing at (a) 1000 and (b) 1400 UTC 23 Nov 1981.

because the zone of wind shift across the front broadened in association with a weaker pressure trough (Figs. 5b,c and 10b). This line of absolute vorticity maxima was between 0.005 and 0.01 s⁻¹ and contained small maxima of 0.01–0.02 s⁻¹, as calculated on the 1-km grid. The line of vorticity moved across Britain with the cold front (Fig. 12); there were maxima in vorticity over Anglesey at 1100 UTC, near Liverpool at about 1200 UTC, and in southeast England at 1500–1600 UTC, passing southeast of the United Kingdom by 1730 UTC. These times correspond within about an hour of reported tornado times (Rowe and Meaden 1985), which is all that can be expected given that the resolution of the tornado reports is only hourly, providing additional faith in the ability of the simulation to reproduce observed features of the front.

An examination of the three ingredients for deep moist convection [lift, moisture, and instability; e.g., Johns and Doswell (1992)] shows that lift as much as several meters per second was present (not shown), associated with the strong convergence along the cold front inferred from the wind field (Fig. 11b). Moisture and instability can be diagnosed by CAPE (determined from the parcel with the maximum equivalent potential temperature in the column) (Fig. 13). At 1000 UTC, CAPE appeared as patchy areas east of the front but was, generally, less than 50 J kg⁻¹ (Fig. 13a). By 1400 UTC, CAPE increased ahead of the front, with widespread areas over 25 J kg⁻¹ and localized maxima approaching 125 J kg⁻¹, forming a slightly curved narrow (40–70 km wide) crescent of CAPE ahead of the front (Fig. 13b). (Interestingly, a second maximum of CAPE of 25–125 J kg⁻¹ was also

present in a 20–50-km-wide band about 150 km ahead of the front associated with the prefrontal rainband, although this maximum is not part of this story.) Therefore, the three ingredients for deep moist convection (i.e., instability, lift, and moisture) were present along the front.

These large gradients in CAPE occurring over such short distances raise issues about the proximity soundings for U.K. tornadoes. Given that the large gradients in CAPE occur over distances as small as tens of kilometers, this raises questions about the choice of proximity sounding criteria used in Mulder and Schultz (2015) of 180 km and 3 h. Mulder and Schultz (2015) derived their criteria from previous proximity sounding studies in the United States, specifically Brooks (2009). Indeed, the prefrontal sounding for this outbreak in Fig. 8 does not meet these criteria. Other U.K. soundings on that day were even farther away from the tornadoes. Thus, the large variability in CAPE ahead of the front in this case is consistent with the recommendations for proximity sounding criteria for significant tornadoes in the United States of a range of 40–80 km and no more than 2 h (Potvin et al. 2010). Potentially noteworthy is the fact that detailed analysis of CAPE and convective inhibition near supercells in the central United States shows variations of hundreds of joules per kilogram over distances as small as a few kilometers (e.g., Markowski et al. 2002). Therefore, perhaps our results of such strong gradients over tens of kilometers should not be too surprising.

Given the reasonable timing and structure of the modeled front compared to the observations, we can

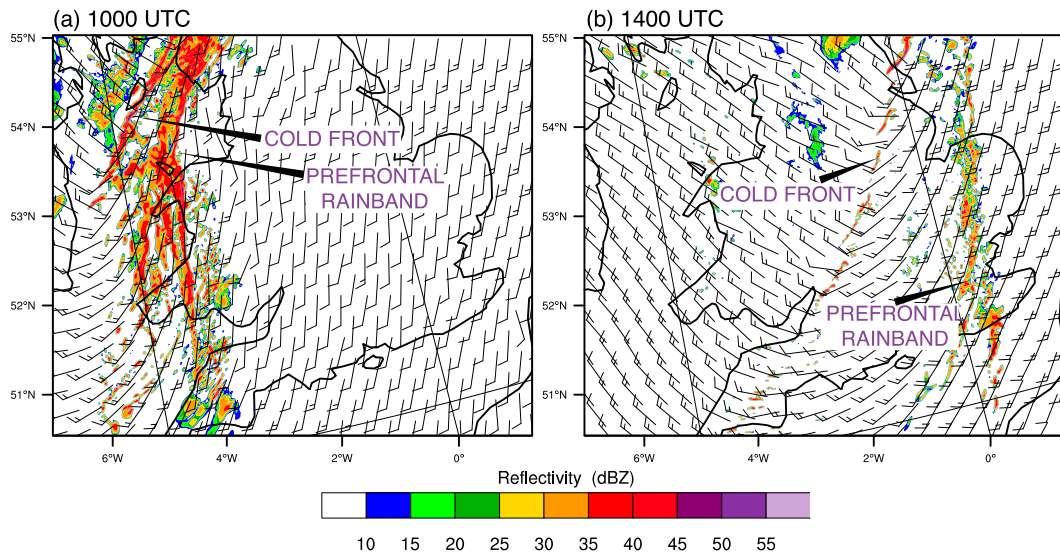


FIG. 11. As in Fig. 10, but for simulation of radar reflectivity factor (dBZ; colored according to scale) and surface winds.

interrogate the model output to determine the reasons that the tornado reports occurred within a relatively narrow swath along the front. Given the existence of organized deep moist convection, the potential for tornadogenesis can be explored with plots of lifting condensation level (LCL), 0–1-km wind shear, and 0–1-km storm-relative helicity. These are quantities known for their ability to discriminate tornadic from nontornadic storms in the United States (e.g., Rasmussen and Blanchard 1998; Thompson et al. 2003, 2012; Craven and Brooks 2004) and Europe (e.g., Púčik et al. 2015; Mulder and Schultz 2015).

At 1000 UTC, the lowest LCL along the front was between 600 and 1000 m (Fig. 14a). By 1400 UTC, the LCL had dropped along a similar crescent-shaped spatial distribution of low LCL (200–600 m) in the south with patches less than 200 m, and significantly higher LCL (greater than 2200 m) behind the front and to the north along the front (Fig. 14b). These results are consistent with conditions for tornadoes in the United Kingdom. Specifically, Mulder and Schultz (2015) found that low LCL height was a statistically significant factor in predicting tornado formation in the United Kingdom, with outbreaks having a mean LCL of about 700 m, as opposed to a null set of convective storms with lightning or hail that had an LCL of 900 m. Therefore, we would expect tornadic storms to be found along the line toward the south where the LCL is lower and the CAPE is higher.

The vertical shear of the horizontal wind over the surface–1-km layer (i.e., 0–1-km wind shear) displayed a sharp change in magnitude across the front (Fig. 15). Just ahead of the front in the swath where the tornadoes

formed, the shear was $10\text{--}20\text{ m s}^{-1}$, with values over 30 m s^{-1} in the prefrontal rainband (Fig. 15b). Behind the front, the shear was only around $5\text{--}10\text{ m s}^{-1}$. Storm-relative helicity over 0–1 km also showed rather large values ahead of the front (Fig. 16). In the immediate vicinity of the front in the prefrontal environment, 0–1-km storm-relative helicity ranged from zero to several hundred meters squared per second squared (Fig. 16).

Thus, despite the cold front extending across nearly the entirety of the United Kingdom (Figs. 5b,c), the narrow swath of tornado reports occurred in what was apparently a sweet spot for the conditions favoring deep moist convection and tornadogenesis along squall lines. Specifically, the swath of tornado reports in this case was limited on the poleward side by the rapidly increasing LCL heights and decreasing CAPE and limited on the equatorward side by the rapidly decreasing absolute vorticity along the cold front, in a prefrontal environment with adequate low-level wind shear and storm-relative helicity all along the front. Although forecasting tornadoes along linear convective systems remains a challenging forecasting problem, this sweet spot may provide insight into providing more specificity for nowcasting tornado development along future linear convective systems in the United Kingdom or elsewhere.

6. Model simulation: Misovortex structure and evolution

The majority of tornado reports occurred within the model domain with 200-m horizontal grid spacing as the modeled front passed through this domain between 1300

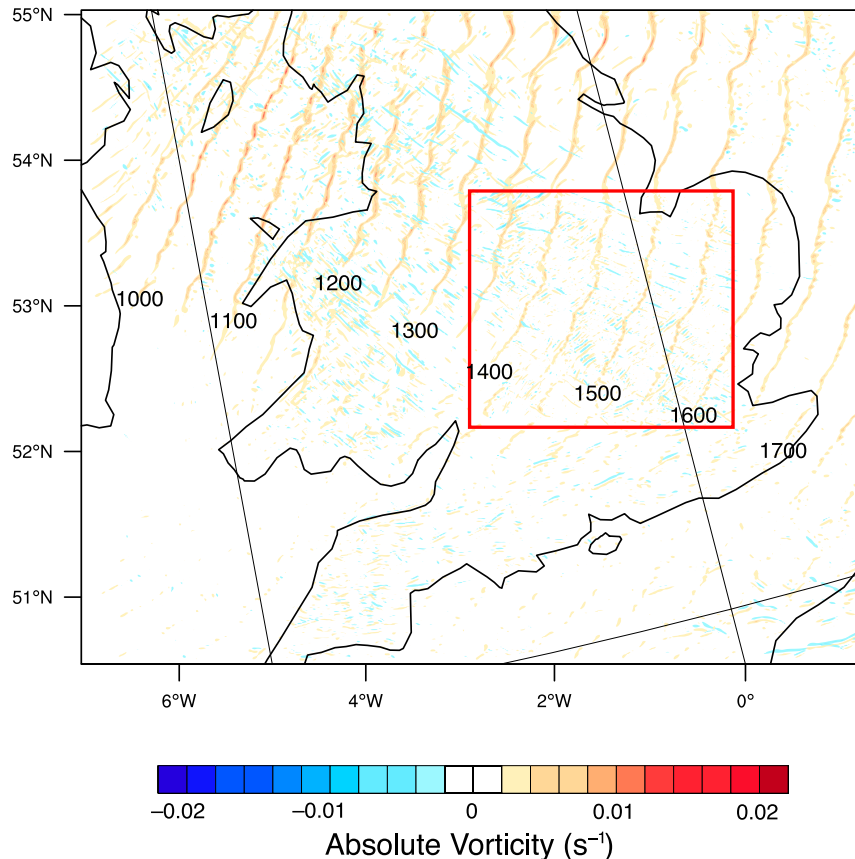


FIG. 12. Simulation of absolute vorticity at 500 m ASL (s^{-1} ; colored according to scale) every 30 min from 0900 to 1800 UTC (labeled every hour) on the domain with 1-km horizontal grid spacing. The red box indicates the location of the domain with 200-m horizontal grid spacing.

and 1640 UTC (Fig. 12). Analysis of vorticity, reflectivity, and surface winds from this domain exhibits more detail along the front where the majority of tornado reports occurred. This region is also where this apparent sweet spot favorable for tornadogenesis occurred.

At this higher resolution, more detail in the structure and evolution of the misovortices is apparent. Specifically, regions of larger 500-m absolute vorticity ($0.02\text{--}0.03\text{ s}^{-1}$) developed into maxima of $0.035\text{--}0.04\text{ s}^{-1}$ within the line, with 500-m updrafts of $5\text{--}10\text{ m s}^{-1}$ (e.g., Fig. 17). Pairing of absolute vorticity maxima and minima was common both within the line and in a few patches slightly ahead of the line, where there was some higher reflectivity as well. Some merging and splitting of downdrafts and maxima, which has been shown to increase vorticity (Lee and Wilhelmson 1997a), was observed, as well. Background reflectivity of 35–45 dBZ occurred within the rainband, with some patches of higher reflectivity of 50–55 dBZ. Similar to the core-and-gap structures observed by Mulder (2015), the shapes of the misovortices at their maximum intensity are quite

similar to each other, specifically, an updraft (usually $5\text{--}10\text{ m s}^{-1}$) located poleward of the misovortex and a downdraft ($3\text{--}6\text{ m s}^{-1}$, although some downdrafts were as large as $6\text{--}9\text{ m s}^{-1}$) located equatorward of the misovortex.

Where the rainband looked like a hook or breaking wave at its edge, the misovortex was typically located at the rear edge of the rainband in the area of lower reflectivity (10–15 dBZ) and, eventually, developed a hook shape (Fig. 18). Many misovortices intensified at the center of the rainband and weakened as they moved backward relative to the rainband, leaving the misovortices on the cold side. Some evolved from a line of vorticity that curled up and split into two hooks, often described as a broken S (McAvoy et al. 2000; Clark 2011), signatures similar to the line-echo wave pattern (Nolen 1959) and the frontal type of misovortices observed in squall lines (Jewett and Wilhelmson 2006). The hook-shaped echo is likely a response to the circulation around the misovortex. The kinematics of misovortices appear to be similar to that of supercells and may suggest that tornadoes along lines may form similar

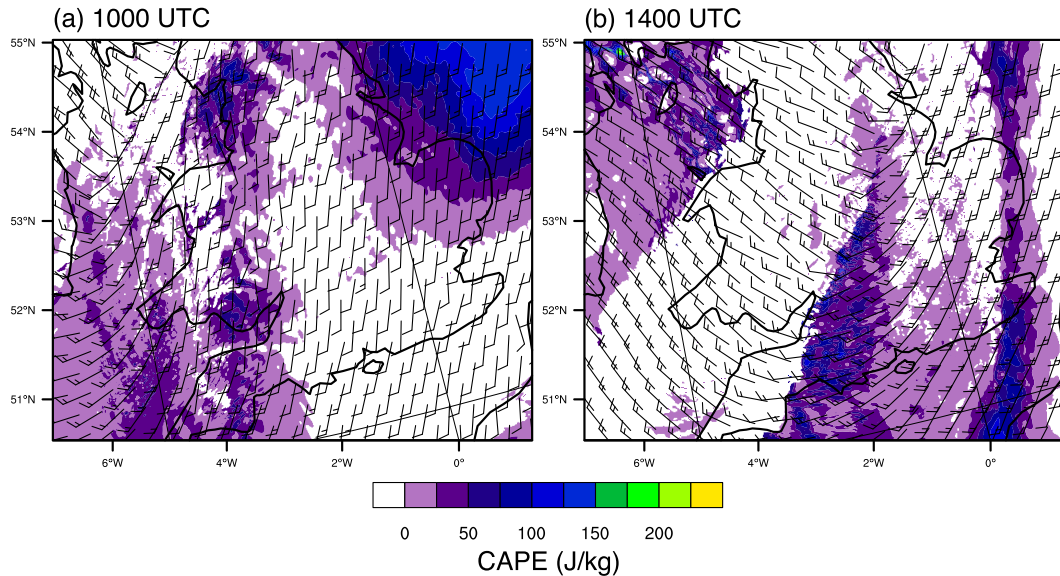


FIG. 13. As in Fig. 10, but for simulation of CAPE (J kg^{-1} ; colored according to scale) and surface winds.

to that inside a supercell, as suggested by Weisman and Trapp (2003). Further investigation is required to confirm whether the dynamics are similar.

To estimate how important these hook-shaped cells were in the model, all the misovortices with absolute vorticity greater than 0.02 s^{-1} were plotted every minute between 1350 and 1450 UTC over the 200-m domain when the front was in the plotted area of Fig. 12 ($110 \text{ km} \times 70 \text{ km}$). Previous simulations of vortices in different storm types have produced vortices of about this magnitude. For supercells, Adlerman et al. (1999) found vorticity of up to 0.054 s^{-1} . For bow echoes,

vorticity magnitudes ranged from 0.009 to 0.02 s^{-1} (Weisman and Trapp 2003; Trapp and Weisman 2003; Wheatley and Trapp 2008; Atkins and St. Laurent 2009). For narrow cold-frontal rainbands, Smart and Browning (2009) found vorticity of up to 0.04 s^{-1} . Although the modeled vorticity magnitudes depend on the case, they also depend on model grid spacing with higher-resolution models producing higher vorticity values. We determined that 0.02 s^{-1} was a good balance between choosing a smaller value with vorticity maxima everywhere and choosing a higher value with relatively few vorticity maxima. If the numbers of vortices and

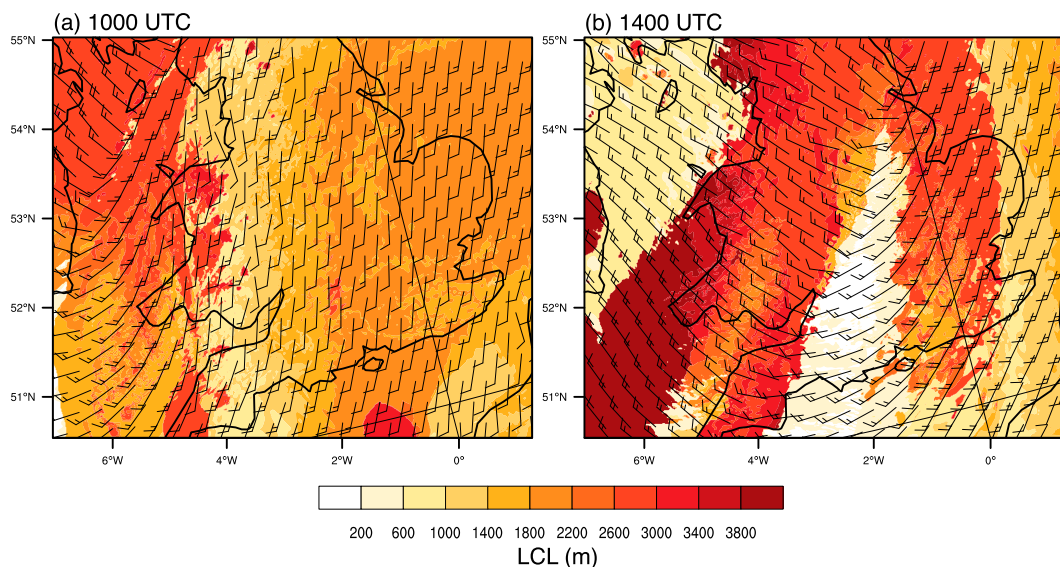


FIG. 14. As in Fig. 10, but for simulation of LCL (m; colored according to scale) and surface winds.

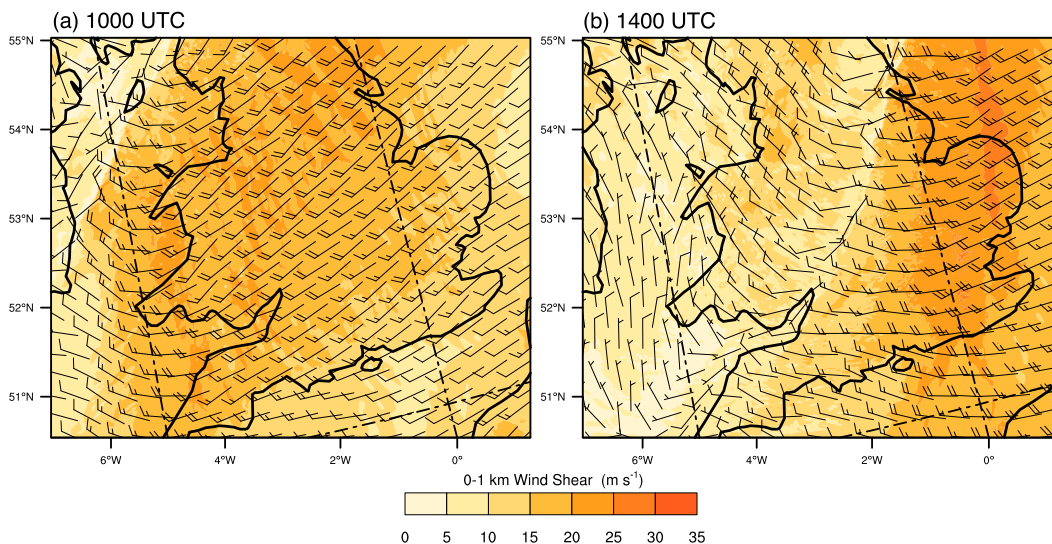


FIG. 15. As in Fig. 10, but for simulation of 0–1-km vertical shear of the horizontal wind in magnitude (m s^{-1} ; colored according to scale) and direction.

vortices with hooks are calculated every 10 min during that 60-min period (seven times), then an average of 39 (with a standard deviation of 3) misovortices existed, of which 20.4% (with a standard deviation of 2.6%) displayed hooks at any one time. Thus, this evolution is relatively common within the model simulation.

7. Reassessment of the number of reports

We can use the simulation, in conjunction with a reexamination of the reports, to reexamine this event.

First, according to the TORRO database, 58 of these reports (56% of the 104 reports) were later verified by TORRO experts, and classified as definite by them; the other 46 reports were deemed to show reasonable evidence of a tornado having occurred, but not enough to be certain; these were classified as probable. So, the minimum number of credible tornadoes was deemed to be 58.

Second, the remaining 46 probable tornado reports were examined for likely duplicate reports. The following approach was employed. Each of the 46 probable

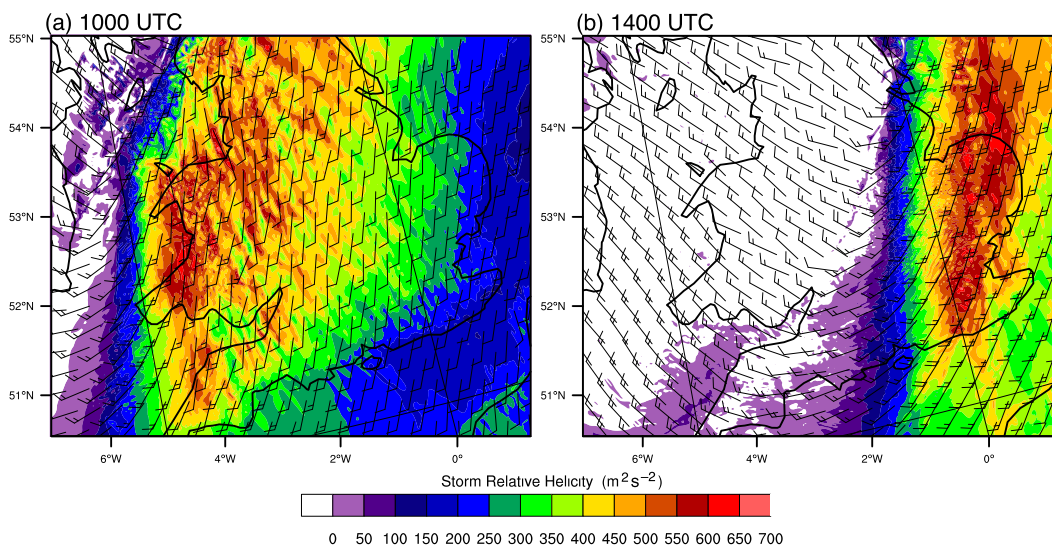


FIG. 16. As in Fig. 10, but for simulation of 0–1-km storm-relative helicity ($\text{m}^2 \text{s}^{-2}$; colored according to scale) and surface winds.

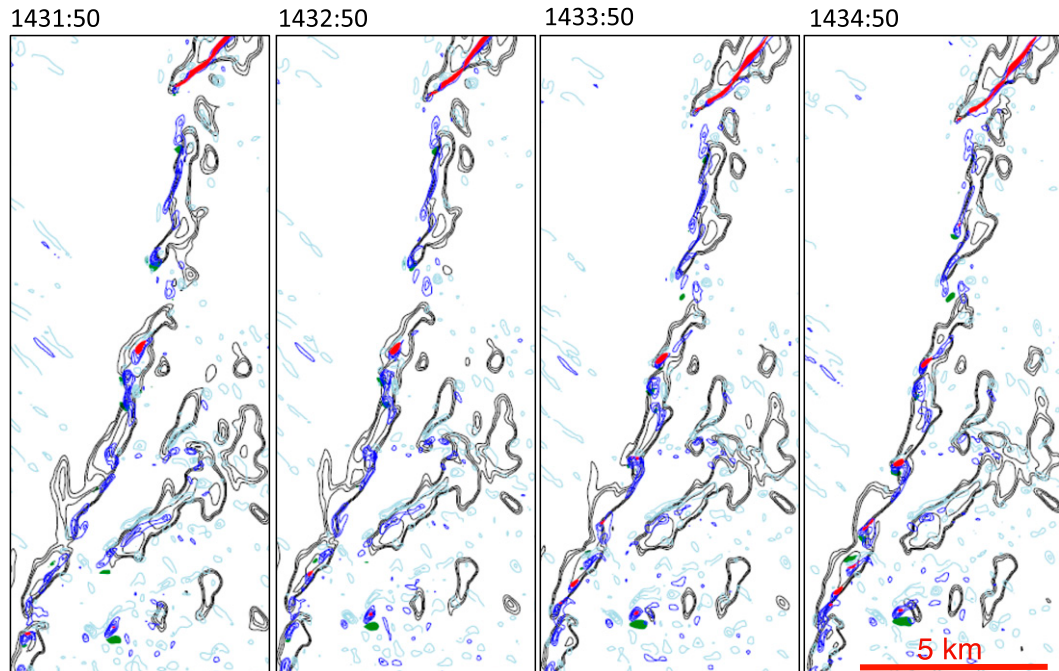


FIG. 17. Simulation of radar reflectivity factor (black lines every 10 dBZ), absolute vorticity at 500 m ASL (positive values are contoured in dark blue solid lines every 0.005 s^{-1} , starting from 0.01 s^{-1} ; negative values are contoured in light blue solid lines every -0.005 s^{-1}), 500-m updrafts (red fill above 5 m s^{-1}), and 500-m downdrafts (green fill above 2 m s^{-1}) from the 200-m horizontal grid-spacing domain, plotted every minute from 1431:50 to 1434:50 UTC 23 Nov 1981.

reports was checked to see if it might have duplicated another report. Duplicate reports were defined in this article as those reports occurring close in space and time, generally 5 km or closer and reported at the same time. Because the reports in the TORRO database are recorded by the hour, in practice this meant tornadoes reported during the same hour. If the duplicate probable report overlapped with a definite report, then the definite report was retained and the probable report was discarded. If a definite tornado report with unknown intensity was combined with a probable tornado report with known intensity, then the intensity was assigned to the single definite report. If the duplicate probable

report overlapped with another probable report, then the more trustworthy probable report was retained and the other report was discarded. Those reports that had been checked by TORRO experts or were possessing tornado tracks, direction of travel, or high T-scale value were deemed to be the most trustworthy and retained. This check reduced the number of probable reports by 14 to 32. These two checks reduced the number of tornadoes on 23 November 1981 to as few as 58 and as many as 90 tornadoes (Fig. 19).

Does the simulation provide support for this many tornadoes? The innermost model domain over a section of southeast England contained a subset of 52 of the 104

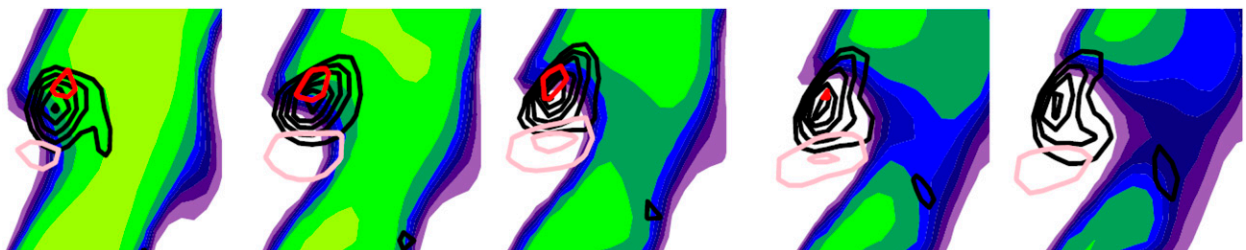


FIG. 18. Characteristic structure and evolution of a simulated misovortex within the domain at 200-m horizontal grid spacing, plotted every 60 s around the time that it matures: radar reflectivity factor (dBZ; colored according to scale in Fig. 16), absolute vorticity at 500 m ASL (black contours every 0.005 s^{-1} , starting from 0.01 s^{-1}), 500-m updraft (red contours every 5 m s^{-1}), and 500-m downdraft (pink contours every 2 m s^{-1}). Each panel is about $4 \text{ km} \times 4 \text{ km}$, and the vortex is about 500 m across.

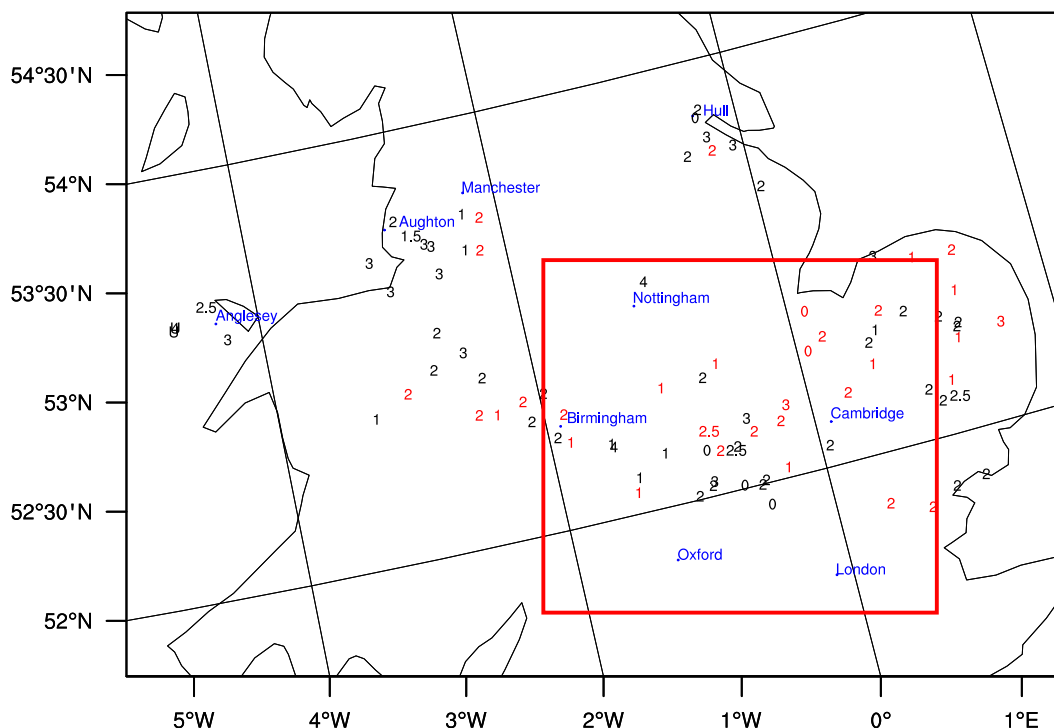


FIG. 19. Locations of the 90 revised tornado reports from the TORRO database for 23 Nov 1981. Numbers represent their strength on the T scale. Reports verified by TORRO (58) are classified as definite and plotted in black. Reports that have not been verified (32) are classified as probable and are plotted in red. Locations discussed in the text are labeled in blue. The red box indicates the location of the domain with 200-m horizontal grid spacing. Locations of reports that appear to be located over water are a result of a coarse representation of geography.

reports and included part of the area targeted by Anglia Television with their 30 reports, which is why this area had a relatively high percentage of probable reports (e.g., Fig. 1). The reexamination above reduced these 52 reports to 42 tornadoes (22 definite and 20 probable tornadoes).

To produce tracks of these misovortices that might be parent circulations for tornadoes, absolute vorticity greater than 0.02 s^{-1} was plotted every minute over the 200-m domain (Fig. 20a). Taking 30 min (± 2 min because the data interval is every minute) as an approximate minimum lifetime for a parent misovortex to produce a tornado (e.g., Wakimoto and Wilson 1989; Brady and Szoke 1989), the number of misovortices produced by the model was counted. This plot was repeated for absolute vorticity maxima greater than 0.025 s^{-1} , updrafts greater than 5, 6, and 7 m s^{-1} , and downdrafts greater than 2, 3, and 4 m s^{-1} (Fig. 20). The results of counting these tracks are summarized in Table 1, which includes the average and median duration of tracks lasting 30 min or more (termed long lived), and the longest duration and track lengths. These results show a substantial number of long-lived tracks of various intensities (e.g., nine misovortices of 0.025 s^{-1} or more, 23 updrafts of 5 m s^{-1} or more, 10

downdrafts of 2 m s^{-1} or more). Most of the model tracks were from the northwest (note the line of constant longitude in the panels in Fig. 20), consistent with the TORRO reports of tracks being mostly from the northwest. A few tracks from the west or southwest, however, were also present (e.g., Figs. 20a,c), which was also consistent with a few of the tornado reports.

Although some of the tracks of misovortices with vorticity greater than or equal to 0.02 s^{-1} on the 200-m grid are within 5 km of each other, tornado reports less than 5 km apart are more likely to represent the same tornado than ones say 20 km apart. We can never claim that our approach is perfect but merely suggests a plausible way to filter possibly duplicate reports. Also, there was some ambiguity in how the locations of the reports were recorded (which may have been as specific as the name of a town, rather than a quantitative latitude–longitude coordinate). Such ambiguities would complicate the assessment of the duplicate reports. Finally, the tornado reports that were discounted were listed as only probable by TORRO, so there is no risk of eliminating definite tornadoes. Thus, we are confident in the model's ability to produce a large number of misovortices that are consistent with the large number

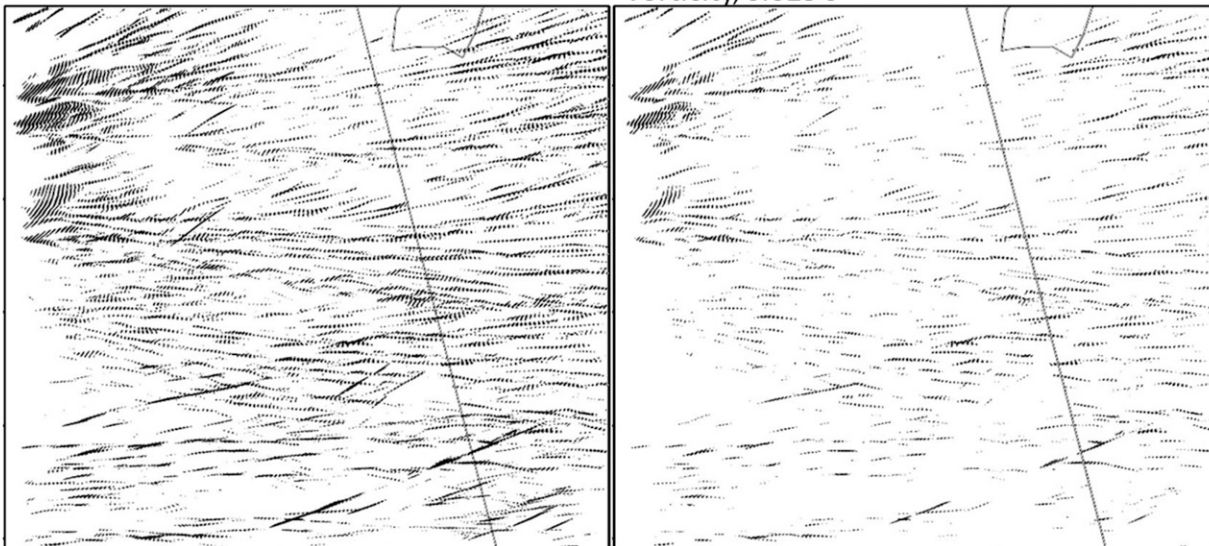
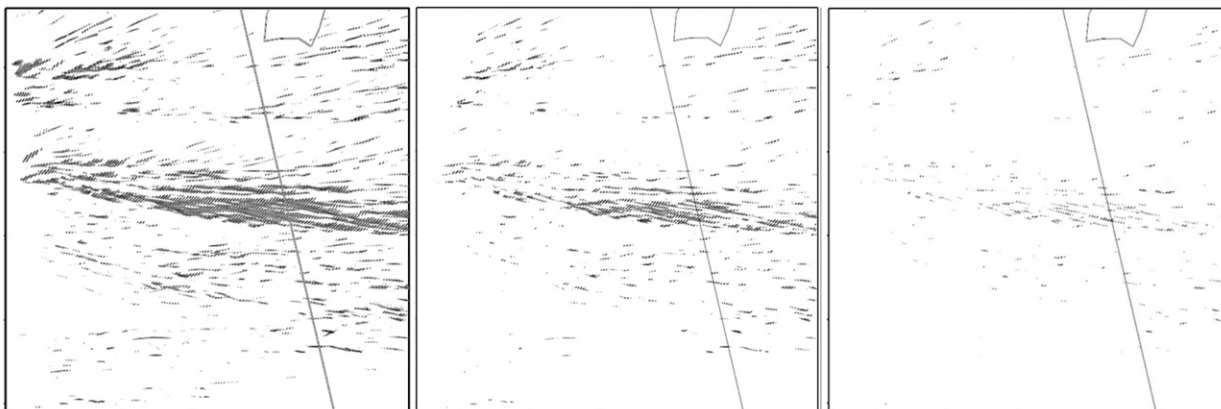
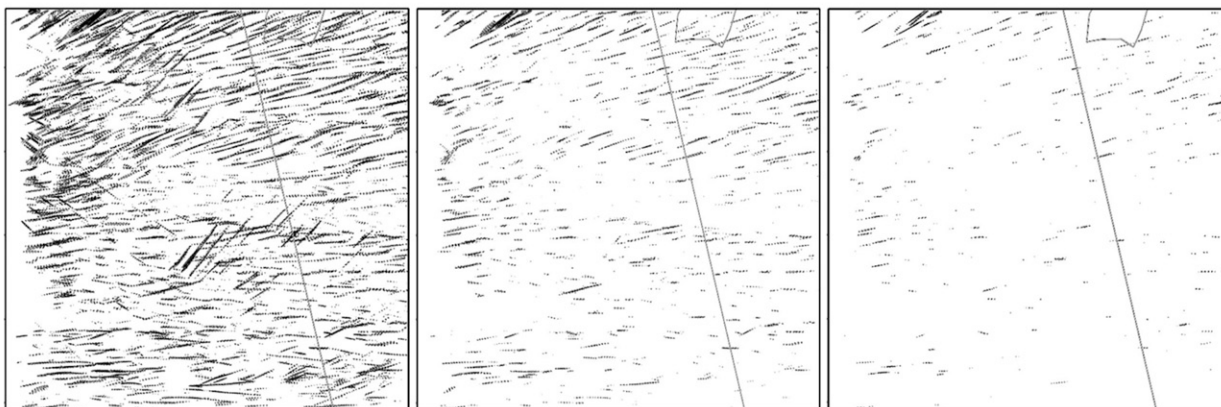
a. Vorticity, 0.02 s^{-1} Vorticity, 0.025 s^{-1} b. Updrafts, 5 m s^{-1} Updrafts, 6 m s^{-1} Updrafts, 7 m s^{-1} c. Downdrafts, 2 m s^{-1} Downdrafts, 3 m s^{-1} Downdrafts, 4 m s^{-1} 

FIG. 20. Tracks of (a) 500-m absolute vorticity (0.02 and 0.025 s^{-1}), (b) 500-m updrafts (5 , 6 , and 7 m s^{-1}), and (c) 500-m downdrafts (2 , 3 , and 4 m s^{-1}) plotted every minute from 1300 to 1600 UTC in the domain with 200-m horizontal grid spacing.

TABLE 1. Properties of tracks of 500-m absolute vorticity (0.02 and 0.025 s^{-1}), updrafts (5 , 6 , and 7 m s^{-1}), and downdrafts (2 , 3 , and 4 m s^{-1}) in the domain with 200-m horizontal grid spacing between 1300 and 1600 UTC. “Long lived” refers to features lasting 30 min or more (± 2 min because the data interval is every minute). The longest duration track being listed as “101+” means that a track started within the plotting domain but continued to the edge of the domain, indicating that the track could have existed longer than 101 min. N/A represents no features meeting the designated criteria.

	No. of long-lived maxima	Avg duration of long-lived tracks (min)	Median duration of long-lived tracks (min)	Longest duration track (min)	Longest track length (to nearest 5 km)
Vorticity ($>0.02 \text{ s}^{-1}$) tracks	41	40.3	37	64	75
Vorticity ($>0.025 \text{ s}^{-1}$) tracks	9	33.2	33	38	45
Updraft ($>5 \text{ m s}^{-1}$) tracks	23	55.3	48	101+	175
Updraft ($>6 \text{ m s}^{-1}$) tracks	5	54.2	56	76	100
Updraft ($>7 \text{ m s}^{-1}$) tracks	0	N/A	N/A	28	35
Downdraft ($>2 \text{ m s}^{-1}$) tracks	10	34.2	33.5	40	75
Downdraft ($>3 \text{ m s}^{-1}$) tracks	0	N/A	N/A	22	35
Downdraft ($>4 \text{ m s}^{-1}$) tracks	0	N/A	N/A	12	20

of tornado reports widespread over a large region of England and Wales.

If the tornadoes on this day developed from parent misovortices that were formed by the tilting-shear mechanism (e.g., Trapp and Weisman 2003), we would expect horizontal vorticity to develop first, increase, be tilted vertically by an updraft–downdraft dipole, and then weaken. Thus, we would expect the parent misocyclone to have a shorter lifetime than the updraft. From Fig. 20 and Table 1, examples of tracks of updrafts (5 – 10 m s^{-1})

and tracks of vorticity greater than 0.02 s^{-1} had similar lengths. The vorticity increased to above 0.025 s^{-1} along the tracks and then toward the end of the tracks. Downdrafts of 3 – 6 m s^{-1} also appeared alongside these tracks for shorter lengths than the updrafts and of only slightly shorter lengths than the higher-vorticity tracks. Counting the number of absolute vorticity maxima of 0.02 s^{-1} or more that last for 30 min or longer yields 41 misovortices, with some of the longer-lasting updrafts forming multiple misovortices. Of these 41 misovortices, 30 have updrafts

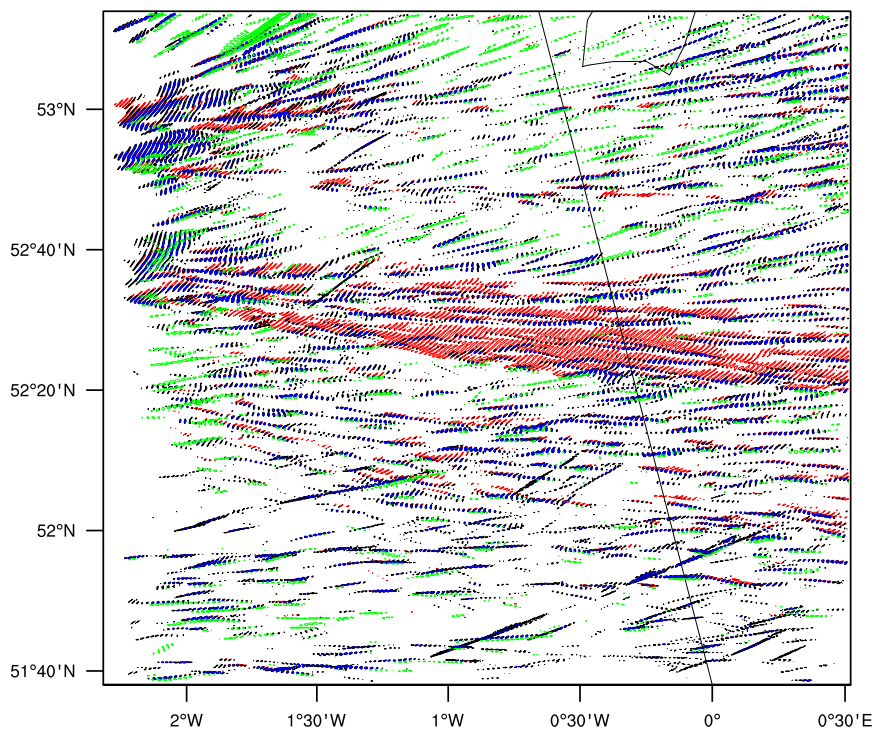


FIG. 21. Simulation of 0.02 and 0.025 s^{-1} absolute vorticity at 500 m ASL (black contours), 5 m s^{-1} updrafts at 500 m (red contours), and 3 m s^{-1} downdrafts at 500 m (green contours) plotted every minute from 1300 to 1600 UTC on the domain with 200-m horizontal grid spacing.

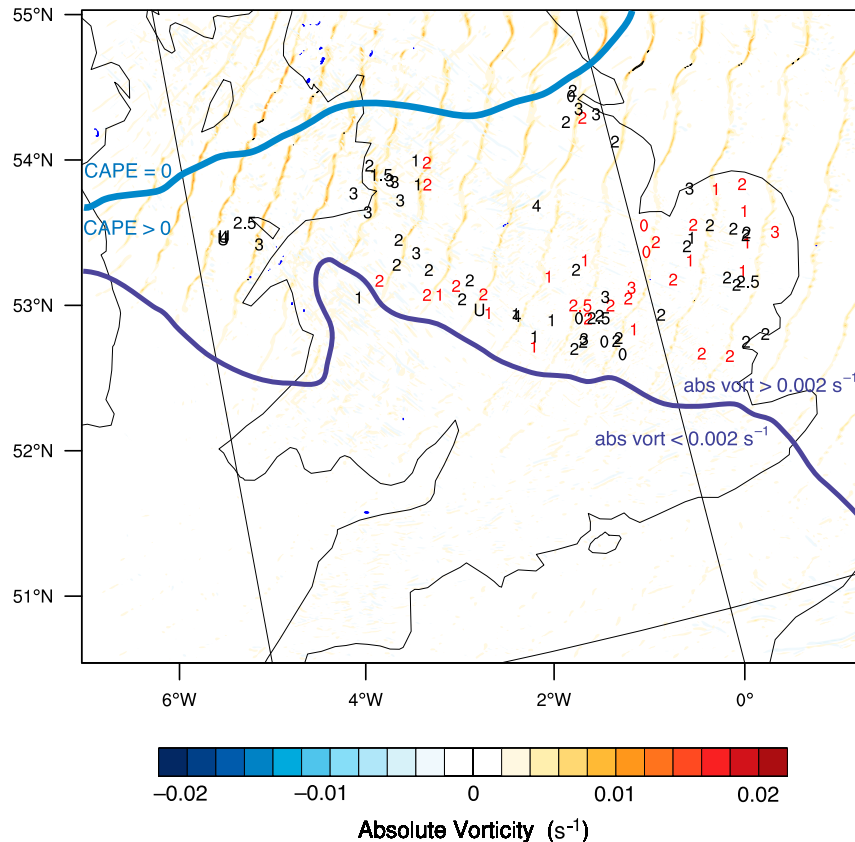


FIG. 22. Simulation of absolute vorticity at 500 m ASL (s^{-1} ; colored according to scale) every 30 min from 0900 to 1800 UTC on the domain with 1-km horizontal grid spacing. Purple lines separate approximate areas with simulated absolute vorticity less than 0.002 s^{-1} on the 1-km domain during the time of frontal passage. Blue lines separate approximate areas with simulated positive CAPE during the time of frontal passage. Locations of reports that appear to be located over water are a result of a coarse representation of geography. Locations of the 90 tornado reports from the TORRO database for 23 Nov 1981. Numbers represent their strength on the T scale. Reports verified by TORRO (58) are classified as definite and plotted in black. Reports that have not been verified (32) are classified as probable and are plotted in red.

of 5 m s^{-1} or more and downdrafts of 3 m s^{-1} or more each lasting longer than 4 min, meaning that there are roughly 30 possible parent circulations in the 200-m domain alone (Fig. 21). Of these 30 tracks, the average lifetime of the tracks was 47.6 min (median of 39 min), and the longest track was 175 km and lasted for 109 min. When linked with favorable environmental conditions for tornadogenesis in the model and the results of Atkins et al. (2004), who found that tornadoes were more likely to form from parent misovortices along the convective line that had greater rotation rates, the potential existed for the model misovortices to have been tornadic. Thus, these roughly 30 intense misovortices within the innermost domain are sufficient to explain the 22–44 tornado reports within this domain.

Figure 22 combines the half-hourly absolute vorticity isochrones with the regions with favorable CAPE and

vorticity values, and the observed 90 tornado reports. The majority of the tornado reports (89 out of 90) were within the favorable locations (high vorticity along the cold front and nonzero CAPE). Also, there was agreement between the modeled misocyclone tracks and the locations of the tornado reports, providing additional veracity of the simulation. The possibility also existed that these misovortices could have produced multiple tornadoes each. Therefore, these statistics give an indication of the potential of high-resolution modeling to resolve features potentially responsible for the tornadoes, as convection-permitting simulations did 15 years ago for the 3 May 1999 Oklahoma–Kansas supercellular tornado outbreak (e.g., Roebber et al. 2002), and provides justification for a potentially large number of possible parent circulations for tornadogenesis in this event.

8. Conclusions

The U.K. tornado outbreak of 23 November 1981 is analyzed through a convection-permitting model simulation and a reexamination of the 104 tornado reports collected by TORRO. This case has been called Britain's greatest tornado outbreak (Rowe and Meaden 1985) because its 104 reports were so much greater than the next highest outbreak of 29. A synoptic situation with a strong cold front, weak CAPE (less than 125 J kg^{-1}), prefrontal winds nearly parallel to the front, and postfrontal winds nearly perpendicular to the front is consistent with weather conditions associated with other tornado outbreaks in the United Kingdom (Clark 2009; Clark and Parker 2014).

The model simulation produced a narrow cold-frontal rainband along a line of absolute vorticity exceeding 0.02 s^{-1} on the 200-m grid with embedded maxima of $0.035\text{--}0.04 \text{ s}^{-1}$, similar to those in previous simulations of misovortices along cold fronts in the United Kingdom (Smart and Browning 2009). Misovortices along the front formed a variety of different structures and evolutions and may have been parent circulations for the tornadoes. A line of reflectivity along the cold front was characterized by precipitation cores and gaps. Updrafts of $5\text{--}10 \text{ m s}^{-1}$ occurred poleward of these maxima of absolute vorticity, and weaker downdrafts of $3\text{--}6 \text{ m s}^{-1}$ occurred equatorward, suggesting the potential for tilting to be involved in tornadogenesis.

The line of absolute vorticity weakened rapidly to the south in conjunction with a weakened pressure trough. Nearly all of the tornadoes reported occurred within a sweet spot where the absolute vorticity was strong enough (more than 0.002 s^{-1} on the 1-km grid) and the CAPE was positive in an environment that was otherwise favorable for tornadoes (0–1-km storm-relative helicity and 0–1-km shear). This approach suggests a means by which regions favorable for tornadoes along squall lines could be forecast in the United Kingdom and elsewhere. The narrow (tens of kilometers) region of positive CAPE in advance of the front also raises concerns about large distances used in determining proximity soundings in previous studies (100–200 km).

Within the model domain with 200-m horizontal grid spacing, 30 possible parent misovortices were present with the following characteristics: absolute vorticity greater than 0.02 s^{-1} , updrafts between 5 and 10 m s^{-1} for longer than 30 min, and downdrafts between 3 and 6 m s^{-1} were present for at least 4 min. This number of parent misovortices was comparable to the figure of 22–44 tornado reports in this area. We conclude that the number of reports in this area was potentially credible.

Reassessing the quality, timing, and location of the reports allows us to place revised boundaries on the

lower and upper limits of the number of tornadoes that day. A final figure was produced of 90 tornadoes: 58 definite and 32 probable, a slight reduction from the 104 total reports. This revision does not eliminate the problem of the event distorting the historical record (Mulder and Schultz 2015; Antonescu et al. 2016). Even if the lower limit were closer to 58 reports, this event would still be the largest documented tornado outbreak in the United Kingdom.

Acknowledgments. We thank TORRO, in particular Terence Meaden and Paul Brown, for providing the tornado data for 23 November 1981, and Jeff Trapp, David Smart, and an anonymous reviewer for their comments that have improved this article. We thank ARCHER, the U.K. National Supercomputing Service, for hosting the simulations. The historical weather maps were provided by Mark Beswick of the National Meteorological Archive and Duncan Ball of the Met Office Library, and we thank Stephen Burt for telling us about the existence of these map archives. The satellite imagery was provided by Andrew Brooks and Neil Lonie of the Dundee Satellite Receiving Station. Jonathan Fairman provided the CAPE value from the NCEP–NCAR reanalysis. Funding for Apsley was provided by the U.K. Natural Environment Research Council through Manchester–Liverpool Doctoral Training Programme Grant NE/L002469/1. Funding for Mulder was provided by a scholarship from the Faculty of Engineering and Physical Sciences, University of Manchester. Partial funding for Schultz was provided by the Natural Environment Research Council to the University of Manchester through Grants NE/H008225/1, NE/I005234/1, and NE/N003918/1 and by the Risk Prediction Initiative of the Bermuda Institute of Ocean Sciences through Grant RPI2.0-2016-SCHULTZ.

REFERENCES

- Adlerman, E. J., K. K. Droegemeier, and R. Davies-Jones, 1999: A numerical simulation of cyclic mesocyclogenesis. *J. Atmos. Sci.*, **56**, 2045–2069, doi:[10.1175/1520-0469\(1999\)056<2045:ANSOCM>2.0.CO;2](https://doi.org/10.1175/1520-0469(1999)056<2045:ANSOCM>2.0.CO;2).
- Antonescu, B., D. M. Schultz, F. Lomas, and T. Kühne, 2016: Tornadoes in Europe: Synthesis of the observational datasets. *Mon. Wea. Rev.*, doi:[10.1175/MWR-D-15-0298.1](https://doi.org/10.1175/MWR-D-15-0298.1), in press.
- Atkins, N. T., and M. St. Laurent, 2009: Bow echo mesovortices. Part I: Processes that influence their damaging potential. *Mon. Wea. Rev.*, **137**, 1497–1513, doi:[10.1175/2008MWR2649.1](https://doi.org/10.1175/2008MWR2649.1).
- , J. M. Arnott, R. W. Przybylinski, R. A. Wolf, and B. D. Ketcham, 2004: Vortex structure and evolution within bow echoes. Part I: Single-Doppler and damage analysis of the 29 June 1998 derecho. *Mon. Wea. Rev.*, **132**, 2224–2242, doi:[10.1175/1520-0493\(2004\)132<2224:VSAEWB>2.0.CO;2](https://doi.org/10.1175/1520-0493(2004)132<2224:VSAEWB>2.0.CO;2).
- Bolton, N., D. M. Elsom, and G. T. Meaden, 2003: Forecasting tornadoes in the United Kingdom. *Atmos. Res.*, **67–68**, 53–72, doi:[10.1016/S0169-8095\(03\)00083-8](https://doi.org/10.1016/S0169-8095(03)00083-8).

- Brady, R. H., and E. J. Szoke, 1989: A case study of nonmesocyclone tornado development in northeast Colorado: Similarities to waterspout formation. *Mon. Wea. Rev.*, **117**, 843–856, doi:10.1175/1520-0493(1989)117<0843:ACSONT>2.0.CO;2.
- Brooks, H. E., 2009: Proximity soundings for severe convection for Europe and the United States from reanalysis data. *Atmos. Res.*, **93**, 546–553, doi:10.1016/j.atmosres.2008.10.005.
- , and C. A. Doswell, 2001: Some aspects of the international climatology of tornadoes by damage classification. *Atmos. Res.*, **56**, 191–201, doi:10.1016/S0169-8095(00)00098-3.
- Brown, M. J., J. D. Locatelli, M. T. Stoelinga, and P. V. Hobbs, 1999: Numerical modeling of precipitation cores on cold fronts. *J. Atmos. Sci.*, **56**, 1175–1196, doi:10.1175/1520-0469(1999)056<1175:NMOPCO>2.0.CO;2.
- Browning, K. A., 1990: Organization of clouds and precipitation in extratropical cyclones. *Extratropical Cyclones: The Erik Palmén Memorial Volume*, C. W. Newton and E. O. Holopainen, Eds., Amer. Meteor. Soc., 129–153.
- , and T. W. Harrold, 1970: Air motion and precipitation growth at a cold front. *Quart. J. Roy. Meteor. Soc.*, **96**, 369–389, doi:10.1002/qj.49709640903.
- , and C. W. Pardoe, 1973: Structure of low-level jet streams ahead of mid-latitude cold fronts. *Quart. J. Roy. Meteor. Soc.*, **99**, 619–638, doi:10.1002/qj.49709942204.
- , and R. Reynolds, 1994: Diagnostic study of a narrow cold frontal rainband and severe winds associated with a stratospheric intrusion. *Quart. J. Roy. Meteor. Soc.*, **120**, 235–257, doi:10.1002/qj.49712051602.
- , and N. M. Roberts, 1996: Variation of frontal and precipitation structure along a cold front. *Quart. J. Roy. Meteor. Soc.*, **122**, 1845–1872, doi:10.1002/qj.49712253606.
- , —, and A. J. Illingworth, 1997: Mesoscale analysis of the activation of a cold front during cyclogenesis. *Quart. J. Roy. Meteor. Soc.*, **123**, 2349–2375, doi:10.1002/qj.49712354410.
- Carbone, R. E., 1982: A severe frontal rainband. Part I: Stormwide hydrodynamic structure. *J. Atmos. Sci.*, **39**, 258–279, doi:10.1175/1520-0469(1982)039<0258:ASFRPI>2.0.CO;2.
- , 1983: A severe frontal rainband. Part II: Tornado parent vortex circulation. *J. Atmos. Sci.*, **40**, 2639–2654, doi:10.1175/1520-0469(1983)040<2639:ASFRPI>2.0.CO;2.
- Clark, M. R., 2009: The southern England tornadoes of 30 December 2006: Case study of a tornadic storm in a low CAPE, high shear environment. *Atmos. Res.*, **93**, 50–65, doi:10.1016/j.atmosres.2008.10.008.
- , 2011: Doppler radar observations of mesovortices within a cool-season tornadic squall line over the UK. *Atmos. Res.*, **100**, 749–764, doi:10.1016/j.atmosres.2010.09.007.
- , 2013: A provisional climatology of cool-season convective lines in the UK. *Atmos. Res.*, **123**, 180–196, doi:10.1016/j.atmosres.2012.09.018.
- , and D. J. Parker, 2014: On the mesoscale structure of surface wind and pressure fields near tornadic and nontornadic cold fronts. *Mon. Wea. Rev.*, **142**, 3560–3585, doi:10.1175/MWR-D-13-00395.1.
- Craven, J. P., and H. E. Brooks, 2004: Baseline climatology of sounding derived parameters associated with deep moist convection. *Natl. Wea. Dig.*, **28**, 13–24.
- Doe, R. K., Ed., 2016: *Extreme Weather: Forty Years of the Tornado and Storm Research Organisation (TORRO)*. Wiley Blackwell, 327 pp.
- Elsom, D. M., G. T. Meaden, D. J. Reynolds, M. W. Rowe, and J. D. C. Webb, 2001: Advances in tornado and storm research in the United Kingdom and Europe: The role of the Tornado and Storm Research Organisation. *Atmos. Res.*, **56**, 19–29, doi:10.1016/S0169-8095(00)00084-3.
- Fujita, T., 1981: Tornadoes and downbursts in the context of generalized planetary scales. *J. Atmos. Sci.*, **38**, 1511–1534, doi:10.1175/1520-0469(1981)038<1511:TADITC>2.0.CO;2.
- Groenemeijer, P., U. Corsmeier, and Ch. Kottmeier, 2011: The development of tornadic storms on the cold side of a front favoured by local enhancement of moisture and CAPE. *Atmos. Res.*, **100**, 765–781, doi:10.1016/j.atmosres.2010.10.028.
- Hagen, M., 1992: On the appearance of a cold front with a narrow rainband in the vicinity of the Alps. *Meteor. Atmos. Phys.*, **48**, 231–248, doi:10.1007/BF01029571.
- Hobbs, P. V., and K. R. Biswas, 1979: The cellular nature of narrow cold-frontal rainbands. *Quart. J. Roy. Meteor. Soc.*, **105**, 723–727, doi:10.1002/qj.49710544516.
- , and P. O. G. Persson, 1982: The mesoscale and microscale structure and organization of clouds and precipitation in midlatitude cyclones. Part V: The substructure of narrow cold-frontal rainbands. *J. Atmos. Sci.*, **39**, 280–295, doi:10.1175/1520-0469(1982)039<0280:TMAMSA>2.0.CO;2.
- Holden, J., and A. Wright, 2004: Tornado climatology and the development of simple prediction tools. *Quart. J. Roy. Meteor. Soc.*, **130**, 1009–1021, doi:10.1256/qj.03.45.
- Houze, R. A., Jr., 2014: *Cloud Dynamics*. 2nd ed. Academic Press, 496 pp.
- James, P. K., and K. A. Browning, 1979: Mesoscale structure of line convection at surface cold fronts. *Quart. J. Roy. Meteor. Soc.*, **105**, 371–382, doi:10.1002/qj.49710544404.
- Janjić, Z. I., 1994: The step-mountain eta coordinate model: Further developments of the convection, viscous sublayer and turbulence closure schemes. *Mon. Wea. Rev.*, **122**, 927–945, doi:10.1175/1520-0493(1994)122<0927:TSMECM>2.0.CO;2.
- , 2002: Nonsingular implementation of the Mellor–Yamada level 2.5 scheme in the NCEP Meso model. NCEP Office Note 437, 61 pp. [Available online at <http://www.emc.ncep.noaa.gov/officenotes/newernotes/on437.pdf>.]
- Jewett, B. F., and R. B. Wilhelmson, 2006: The role of forcing in cell morphology and evolution within midlatitude squall lines. *Mon. Wea. Rev.*, **134**, 3714–3734, doi:10.1175/MWR3164.1.
- Johns, R. H., and C. A. Doswell III, 1992: Severe local storms forecasting. *Wea. Forecasting*, **7**, 588–612, doi:10.1175/1520-0434(1992)007<0588:SLSF>2.0.CO;2.
- Jorgensen, D. P., Z. Pu, P. O. G. Persson, and W. Tao, 2003: Variations associated with cores and gaps of a Pacific narrow cold frontal rainband. *Mon. Wea. Rev.*, **131**, 2705–2729, doi:10.1175/1520-0493(2003)131<2705:VAWCAG>2.0.CO;2.
- Kain, J. S., 2004: The Kain–Fritsch convective parameterization: An update. *J. Appl. Meteor.*, **43**, 170–181, doi:10.1175/1520-0450(2004)043<0170:TKCPAU>2.0.CO;2.
- , and J. M. Fritsch, 1990: A one-dimensional entraining/detraining plume model and its application in convective parameterization. *J. Atmos. Sci.*, **47**, 2784–2802, doi:10.1175/1520-0469(1990)047<2784:AODEPM>2.0.CO;2.
- Kalnay, E., and Coauthors, 1996: The NCEP/NCAR 40-Year Reanalysis Project. *Bull. Amer. Meteor. Soc.*, **77**, 437–471, doi:10.1175/1520-0477(1996)077<0437:TNYRP>2.0.CO;2.
- Kawashima, M., 2011: Numerical study of horizontal shear instability waves along narrow cold frontal rainbands. *J. Atmos. Sci.*, **68**, 878–903, doi:10.1175/2010JAS3599.1.
- Kemp, A. K., and S. J. Morris, 1982: Line squall and minor tornadoes at Holyhead, 23 November 1981. *Meteor. Mag.*, **111**, 253–261.
- Kirk, P. J., 2014: An updated tornado climatology for the UK: 1981–2010. *Weather*, **69**, 171–175, doi:10.1002/wea.2247.

- Kobayashi, F., Y. Sugawara, M. Imai, M. Matsui, A. Yoshida, and Y. Tamura, 2007: Tornado generation in a narrow cold frontal rainband—Fujisawa tornado on April 20, 2006—. *SOLA*, **3**, 21–24, doi:[10.2151/sola.2007-006](https://doi.org/10.2151/sola.2007-006).
- Lee, B. D., and R. B. Wilhelmson, 1997a: The numerical simulation of nonsupercell tornadogenesis. Part I: Initiation and evolution of pretornadic misocyclone and circulations along a dry outflow boundary. *J. Atmos. Sci.*, **54**, 32–60, doi:[10.1175/1520-0469\(1997\)054<0032:TNSONS>2.0.CO;2](https://doi.org/10.1175/1520-0469(1997)054<0032:TNSONS>2.0.CO;2).
- , and —, 1997b: The numerical simulation of nonsupercell tornadogenesis. Part II: Evolution of a family of tornadoes along a weak outflow boundary. *J. Atmos. Sci.*, **54**, 2387–2415, doi:[10.1175/1520-0469\(1997\)054<2387:TNSONT>2.0.CO;2](https://doi.org/10.1175/1520-0469(1997)054<2387:TNSONT>2.0.CO;2).
- , and —, 2000: The numerical simulation of nonsupercell tornadogenesis. Part III: Parameter tests investigating the role of CAPE, vortex sheet strength, and boundary layer vertical shear. *J. Atmos. Sci.*, **57**, 2246–2261, doi:[10.1175/1520-0469\(2000\)057<2246:TNSONT>2.0.CO;2](https://doi.org/10.1175/1520-0469(2000)057<2246:TNSONT>2.0.CO;2).
- Locatelli, J. D., J. E. Martin, and P. V. Hobbs, 1995: Development and propagation of precipitation cores on cold fronts. *Atmos. Res.*, **38**, 177–206, doi:[10.1016/0169-8095\(94\)00093-S](https://doi.org/10.1016/0169-8095(94)00093-S).
- Markowski, P. M., J. M. Straka, and E. N. Rasmussen, 2002: Direct surface thermodynamic observations within the rear-flank downdrafts of nontornadic and tornadic supercells. *Mon. Wea. Rev.*, **130**, 1692–1721, doi:[10.1175/1520-0493\(2002\)130<1692:DSTOWT>2.0.CO;2](https://doi.org/10.1175/1520-0493(2002)130<1692:DSTOWT>2.0.CO;2).
- McAvoy, B. P., W. A. Jones, and P. D. Moore, 2000: Investigation of an unusual storm structure associated with weak to occasionally strong tornadoes over the eastern United States. Preprints, *20th Conf. on Severe Local Storms*, Orlando, FL, Amer. Meteor. Soc., 182–185.
- Meaden, G. T., 1983: The TORRO tornado intensity scale. *J. Meteor.*, **8**, 151–153.
- , S. Kochev, L. Kolendowicz, A. Kosa-Kiss, I. Marcinoniene, M. Sioutas, H. Tooming, and J. Tyrrell, 2007: Comparing the theoretical versions of the Beaufort scale, the T-scale and the Fujita scale. *Atmos. Res.*, **83**, 446–449, doi:[10.1016/j.atmosres.2005.11.014](https://doi.org/10.1016/j.atmosres.2005.11.014).
- Mellor, G. L., and T. Yamada, 1982: Development of a turbulence closure model for geophysical fluid problems. *Rev. Geophys. Space Phys.*, **20**, 851–875, doi:[10.1029/RG020i004p00851](https://doi.org/10.1029/RG020i004p00851).
- Morrison, H., G. Thompson, and V. Tatarskii, 2009: Impact of cloud microphysics on the development of trailing stratiform precipitation in a simulated squall line: Comparison of one- and two-moment schemes. *Mon. Wea. Rev.*, **137**, 991–1007, doi:[10.1175/2008MWR2556.1](https://doi.org/10.1175/2008MWR2556.1).
- Mulder, K. J., 2015: Tornadoes in the British Isles: Climatology, formation environments, and storm dynamics. Ph.D. dissertation, University of Manchester, 96 pp.
- , and D. M. Schultz, 2015: Climatology, storm morphologies, and environments of tornadoes in the British Isles: 1980–2012. *Mon. Wea. Rev.*, **143**, 2224–2240, doi:[10.1175/MWR-D-14-00299.1](https://doi.org/10.1175/MWR-D-14-00299.1).
- Nolen, R. H., 1959: A radar pattern associated with tornadoes. *Bull. Amer. Meteor. Soc.*, **40**, 277–279.
- Potvin, C. K., K. L. Elmore, and S. J. Weiss, 2010: Assessing the impacts of proximity sounding criteria on the climatology of significant tornado environments. *Wea. Forecasting*, **25**, 921–930, doi:[10.1175/2010WAF2222368.1](https://doi.org/10.1175/2010WAF2222368.1).
- Púčik, T., P. Groenemeijer, D. Rýva, and M. Kolář, 2015: Proximity soundings of severe and nonsevere thunderstorms in central Europe. *Mon. Wea. Rev.*, **143**, 4805–4821, doi:[10.1175/MWR-D-15-0104.1](https://doi.org/10.1175/MWR-D-15-0104.1).
- Rasmussen, E. N., and D. O. Blanchard, 1998: A baseline climatology of sounding-derived supercell and tornado forecast parameters. *Wea. Forecasting*, **13**, 1148–1164, doi:[10.1175/1520-0434\(1998\)013<1148:ABCOSD>2.0.CO;2](https://doi.org/10.1175/1520-0434(1998)013<1148:ABCOSD>2.0.CO;2).
- Roebber, P. J., D. M. Schultz, and R. Romero, 2002: Synoptic regulation of the 3 May 1999 tornado outbreak. *Wea. Forecasting*, **17**, 399–429, doi:[10.1175/1520-0434\(2002\)017<0399:SROTM>2.0.CO;2](https://doi.org/10.1175/1520-0434(2002)017<0399:SROTM>2.0.CO;2).
- Rowe, M. W., 1985: Britain's greatest tornadoes and tornado outbreak. *J. Meteor.*, **10**, 212–220.
- , 2016: Tornado extremes in the United Kingdom: The earliest, longest, widest, severest, and deadliest. *Extreme Weather: Forty Years of the Tornado and Storm Research Organization (TORRO)*, R. K. Doe, Ed., Wiley Blackwell, 77–90.
- , and G. T. Meaden, 1985: Britain's greatest tornado outbreak. *Weather*, **40**, 230–235, doi:[10.1002/j.1477-8696.1985.tb06883.x](https://doi.org/10.1002/j.1477-8696.1985.tb06883.x).
- Skamarock, W. C., and Coauthors, 2008: A description of the Advanced Research WRF version 3. NCAR Tech. Note NCAR/TN-475+STR, 113 pp., doi:[10.5065/D68S4MVH](https://doi.org/10.5065/D68S4MVH).
- Smart, D. J., and K. A. Browning, 2009: Morphology and evolution of cold-frontal misocyclones. *Quart. J. Roy. Meteor. Soc.*, **135**, 381–393, doi:[10.1002/qj.399](https://doi.org/10.1002/qj.399).
- Smith, B. T., R. L. Thompson, J. S. Grams, C. Broyles, and H. E. Brooks, 2012: Convective modes for significant severe thunderstorms in the contiguous United States. Part I: Storm classification and climatology. *Wea. Forecasting*, **27**, 1114–1135, doi:[10.1175/WAF-D-11-00115.1](https://doi.org/10.1175/WAF-D-11-00115.1).
- Speheger, D. A., C. A. Doswell III, and G. J. Stumpf, 2002: The tornadoes of 3 May 1999: Event verification in central Oklahoma and related issues. *Wea. Forecasting*, **17**, 362–381, doi:[10.1175/1520-0434\(2002\)017<0362:TTOMEV>2.0.CO;2](https://doi.org/10.1175/1520-0434(2002)017<0362:TTOMEV>2.0.CO;2).
- Sugawara, Y., and F. Kobayashi, 2009: Vertical structure of misocyclones along a narrow cold frontal rainband. *J. Meteor. Soc. Japan*, **87**, 497–503, doi:[10.2151/jmsj.87.497](https://doi.org/10.2151/jmsj.87.497).
- Thompson, G., P. R. Field, R. M. Rasmussen, and W. D. Hall, 2008: Explicit forecasts of winter precipitation using an improved bulk microphysics scheme. Part II: Implementation of a new snow parameterization. *Mon. Wea. Rev.*, **136**, 5095–5115, doi:[10.1175/2008MWR2387.1](https://doi.org/10.1175/2008MWR2387.1).
- Thompson, R. L., R. Edwards, J. A. Hart, K. L. Elmore, and P. Markowski, 2003: Close proximity soundings within supercell environments obtained from the Rapid Update Cycle. *Wea. Forecasting*, **18**, 1243–1261, doi:[10.1175/1520-0434\(2003\)018<1243:CPSWSE>2.0.CO;2](https://doi.org/10.1175/1520-0434(2003)018<1243:CPSWSE>2.0.CO;2).
- , B. T. Smith, J. S. Grams, A. R. Dean, and C. Broyles, 2012: Convective modes for significant severe thunderstorms in the contiguous United States. Part II: Supercell and QLCS tornado environments. *Wea. Forecasting*, **27**, 1136–1154, doi:[10.1175/WAF-D-11-00116.1](https://doi.org/10.1175/WAF-D-11-00116.1).
- Trapp, R. J., and M. L. Weisman, 2003: Low-level mesovortices within squall lines and bow echoes. Part II: Their genesis and implications. *Mon. Wea. Rev.*, **131**, 2804–2823, doi:[10.1175/1520-0493\(2003\)131<2804:LMWSLA>2.0.CO;2](https://doi.org/10.1175/1520-0493(2003)131<2804:LMWSLA>2.0.CO;2).
- , E. D. Mitchell, G. A. Tipton, D. W. Effertz, A. I. Watson, D. L. Andra Jr., and M. A. Magsig, 1999: Descending and nondescending tornadic vortex signatures detected by WSR-88Ds. *Wea. Forecasting*, **14**, 625–639, doi:[10.1175/1520-0434\(1999\)014<0625:DANTVS>2.0.CO;2](https://doi.org/10.1175/1520-0434(1999)014<0625:DANTVS>2.0.CO;2).
- , S. A. Tessendorf, E. S. Godfrey, and H. E. Brooks, 2005: Tornadoes from squall lines and bow echoes. Part I: Climatological distribution. *Wea. Forecasting*, **20**, 23–34, doi:[10.1175/WAF-835.1](https://doi.org/10.1175/WAF-835.1).

- , D. M. Wheatley, N. T. Atkins, R. W. Przybylinski, and R. Wolf, 2006: Buyer beware: Some words of caution on the use of severe wind reports in postevent assessment and research. *Wea. Forecasting*, **21**, 408–415, doi:[10.1175/WAF925.1](https://doi.org/10.1175/WAF925.1).
- Turner, S., D. M. Elsom, and G. T. Meaden, 1986: An outbreak of 31 tornadoes associated with a cold front in southern England on 20 October 1981. *J. Meteor.*, **11**, 37–50.
- Viale, M., R. A. Houze Jr., and K. L. Rasmussen, 2013: Upstream orographic enhancement of a narrow cold-frontal rainband approaching the Andes. *Mon. Wea. Rev.*, **141**, 1708–1730, doi:[10.1175/MWR-D-12-00138.1](https://doi.org/10.1175/MWR-D-12-00138.1).
- Wakimoto, R. M., and J. W. Wilson, 1989: Non-supercell tornadoes. *Mon. Wea. Rev.*, **117**, 1113–1140, doi:[10.1175/1520-0493\(1989\)117<1113:NST>2.0.CO;2](https://doi.org/10.1175/1520-0493(1989)117<1113:NST>2.0.CO;2).
- , and B. L. Bosart, 2000: Airborne radar observations of a cold front during FASTEX. *Mon. Wea. Rev.*, **128**, 2447–2470, doi:[10.1175/1520-0493\(2000\)128<2447:AROOAC>2.0.CO;2](https://doi.org/10.1175/1520-0493(2000)128<2447:AROOAC>2.0.CO;2).
- Weisman, M. L., and R. J. Trapp, 2003: Low-level mesovortices within squall lines and bow echoes. Part I: Overview and dependence on environmental shear. *Mon. Wea. Rev.*, **131**, 2779–2803, doi:[10.1175/1520-0493\(2003\)131<2779:LMWSLA>2.0.CO;2](https://doi.org/10.1175/1520-0493(2003)131<2779:LMWSLA>2.0.CO;2).
- Wheatley, D. M., and R. J. Trapp, 2008: The effect of mesoscale heterogeneity on the genesis and structure of mesovortices within quasi-linear convective systems. *Mon. Wea. Rev.*, **136**, 4220–4241, doi:[10.1175/2008MWR2294.1](https://doi.org/10.1175/2008MWR2294.1).